Final Technical Report
USGS Award Number: G12AP20101

Project Title:
Seismic Hazard from Induced Earthquakes in Arkansas

Stephen P. Horton

Center for Earthquake Research and Information
University of Memphis
3876 Central Ave., Suite 1
Memphis, TN 38152-3050

(901) 678-4896, fax (901) 678-4734,
shorton@memphis.edu

Award Term
Start: June 1, 2012
End: August 31, 2015

Abstract

CERI and the Arkansas Geological Survey installed a six-station array of seismometers during the first week of September, 2010, to record earthquakes anticipated to occur in the vicinity of two newly-activated waste-disposal wells in north-central Arkansas. Between September 23, 2010, and July 2011, a swarm of small- to moderate-size ($\mathbf{M} \leq 4.7$) earthquakes illuminated a previously undetected fault in the middle of our array between the towns of Guy and Greenbrier. Horton (2012) established a plausible hydraulic connection between the injection depths at three waste-disposal wells and the nearby (<5 km) Guy-Greenbrier Fault. He concluded that injection of fluids at these wells is the most probable cause of the current seismicity and that continued injection could trigger a potentially damaging $\mathbf{M}5.6 – 6.0$ earthquake based on the currently observed fault dimensions (13x3.2km). For this proposal we archived all seismic data related to this experiment at the IRIS DMC with network code **7F**, we performed detailed analyses of earthquake locations on the fault during the initiation period, and we modeled pore-pressure diffusion caused by pressurized waste-fluid injection at two nearby wells, comparing the build-up of pressure with the observed initiation and migration of earthquakes.

For the seismicity ananlysis we presented an updated catalog of 17,395 earthquakes that is complete between $0 <= ml <= 4.4$ between August 2010 and October 20, 2010, located using an updated 1D velocity model for the region. The inclusion of the small magnitude events reveals that seismicity starts below the SRE injection well a month earlier than estimated using only md >2 events. During this period of time, the seismicity migrated from north to south enhancing the resolution of three joined sections that form the northern ~7.3km portion of the fault, which plunges southwards. The seismogenic zone covers the lower portion of the Paleozoic sedimentary layers and extends into the crystalline Precambrian basement (~3km < z < 7.5km). We also found earthquake size distribution varies along the fault with most ml>3 events constrained within the basement. A b-value of 1.1 was obtained for the updated catalog during this period with the b-value varying between 1.45 and 0.74 for different clusters of events. The seismicity pattern at depth is coincident with structural geologic features observed within the Fayetteville Shale (at ~1500m depth). Results were reported in the *Seismological Research Letters* by Ogwari et al. (2016) and at two professional meetings; Horton et al. (2013) and Ogwari et al. (2014).

For the second ananlysis, We model pore-pressure diffusion caused by pressurized waste-fluid injection at two nearby wells and then compare the buildup of pressure with the observed initiation and migration of earthquakes during the early part of the 2010–2011 Guy–Greenbrier earthquake swarm. Pore-pressure diffusion is calculated using MODFLOW 2005 that allows the actual injection histories (volume/day) at the two wells to diffuse through a fractured and faulted 3D aquifer system representing the eastern Arkoma basin. The aquifer system is calibrated using the observed water-level recovery following well shut-in at three wells. We estimate that the hydraulic conductivities of the Boone Formation and Arbuckle Group are 2.2×10^{-2} and 2.03×10^{-3} m day^{-1}, respectively, with a hydraulic conductivity of 1.92×10^{-2} m day^{-1} in the Hunton Group when considering 1.72×10^{-3} m day^{-1} in the Chattanooga Shale. Based on the simulated pressure field, injection near the relatively conductive Enders and Guy–Greenbrier faults (that hydraulically connect the Arbuckle Group with the underlying basement) permits pressure diffusion into the crystalline basement, but the effective radius of influence is limited in

depth by the vertical anisotropy of the hydraulic diffusivity. Comparing spatial/temporal changes in the simulated pore-pressure field to the observed seismicity suggests that minimum pore-pressure changes of approximately 0.009 and 0.035 MPa are sufficient to initiate seismic activity within the basement and sedimentary sections of the Guy–Greenbrier fault, respectively. Further, the migration of a second front of seismicity appears to follow the approximately 0.012 MPa and 0.055 MPa pore-pressure fronts within the basement and sedimentary sections, respectively. Results were reported in *Geofluids* by Ogwari and Horton (2016) and presented at four professional meetings; Ogwari and Horton (2013), Ogwari and Horton (2015A and 2015B) and Ogwari and Horton (2016).

Project Results

We performed two analyses for this project.

Part 1: *Characteristics of induced/triggered earthquakes during the startup phase of the Guy–Greenbrier earthquake sequence in North–Central Arkansas*

Paul O. Ogwari, Stephen P. Horton, Scott Ausbrooks

Introduction

We detect and locate 17,395 earthquakes during the startup phase of the Guy-Greenbrier earthquake swarm providing the first catalog complete for ml > 0 earthquakes. The Guy-Greenbrier earthquake swarm is one of the best-recorded cases of induced earthquakes triggered by fluid injection at class 2 underground injection control (UIC) wells. Three seismic stations were installed within 5km of the fault several months prior to the beginning of the swarm (Figure 1 and Table 1) providing exceptional spatial and temporal coverage of the starting phases of seismic activity. With the high resolution catalog, we find a previously undetected startup phase 660 meters west of the Chesapeake SRE well one month prior to the md>2.0 events ~~in the~~ more distant startup area (~4km SW of SRE) previously suggested by Horton (2012). We observe distinct seismically active patches spatially distributed along the Guy-Greenbrier fault that have episodic behavior. In addition we produce earthquake statistics and observe previously undetected seismic activity off the Guy-Greenbrier fault.

Central Arkansas, especially the Arkoma basin, has a long history of scattered earthquake activity including two intense swarms near Enola in 1982 and 2001 (Chiu *et al.* 1984; Rabak *et al.* 2010). Prior to 2009 there were no fluid injection wells in the vicinity and therefore the two Enola sequences are believed to occur naturally. Since the first fluid-waste disposal well associated with the Fayetteville Shale gas play became operational in April 2009 (Table 2), central Arkansas has experienced an increase in the rate of small and moderate earthquakes. The background rate of M>2.9 earthquakes in Arkansas is 1.6 events/yr based on the number of events in the Advanced National Systems Network (ANSS) catalog between 1967 and 2008. Since 2009 the rate of M>2.9 earthquakes has increased to 11 events/yr, most of which occurred during the Guy-Greenbrier earthquake swarm of 2010 – 2011. There have been no earthquakes of mlbg>2 located along the fault since September 2012. However, the seismic activity rate continues to be elevated in the Fayetteville Shale gas play area. After removing all Guy-
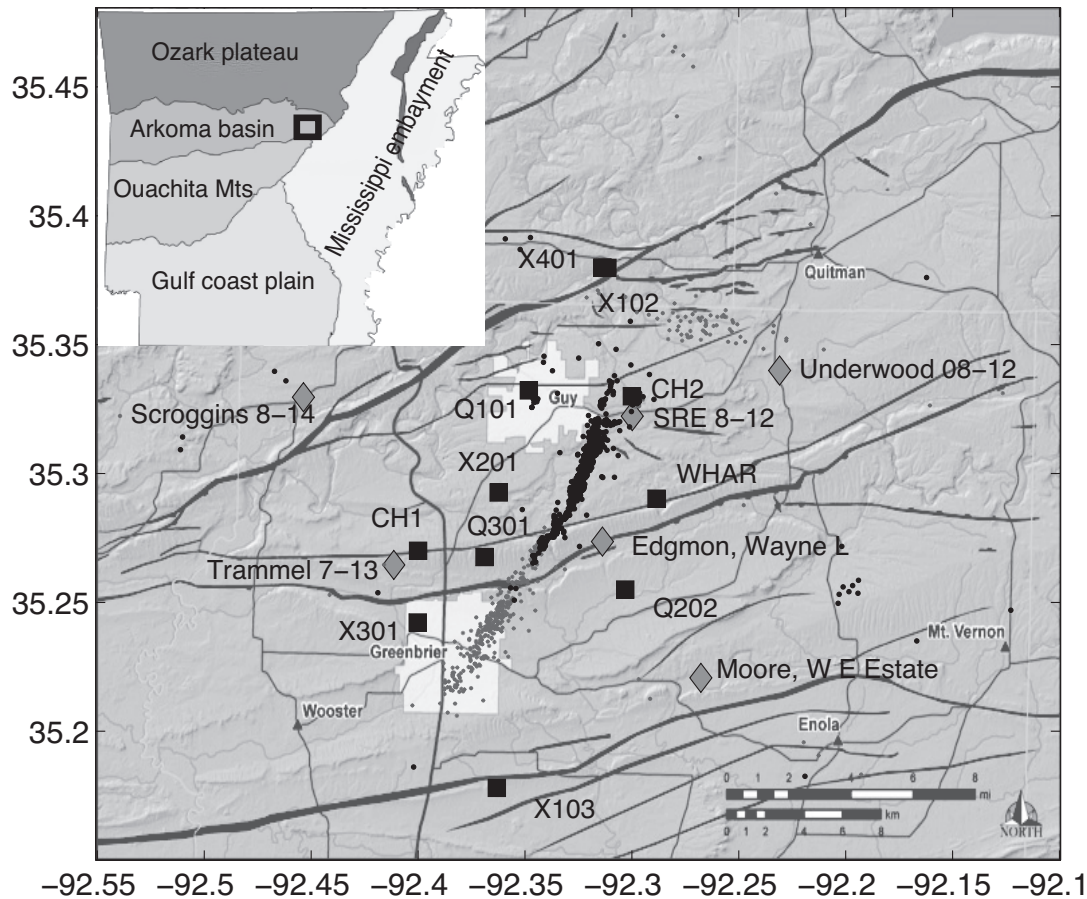
Figure 1: Seismic stations (black square), UIC wells (grey diamond), earthquakes (black) before 02/15/11, and earthquakes (grey) after 02/16/11. Inset: Map of major geological provinces modified from Lancaster (2011) with study area outlined

Greenbrier earthquakes from the rate calculation, the rate of M>2.9 earthquakes in Arkansas since 2009 is 3 events/yr, which is about double the background rate. These earthquakes are both naturally occurring and induced earthquakes that tend to happen in spatial and temporal clusters (Horton *et al.*, 2013).

Horton (2012) showed strong evidence that the Guy-Greenbrier earthquakes were triggered by fluid injection at nearby waste disposal wells. The earthquakes illuminated a previously unknown vertical fault approximately 13km long oriented ~N30°E. The fault is favorably oriented to be critically stressed in a regional stress field dominated by compression along an axis of ~N60-65°E (Zoback and Zoback, 1991) consistent with eastern North America as a whole. The earthquakes occurred within 6km radius of 3 waste disposal wells after the start of injection at those wells (Figure 1) and at shallow depths although below the depth of the injection interval for each well. The earthquakes started within weeks of the beginning of injection at the closest well indicating an existence of hydraulic connection between the injection interval and earthquake depth. The earthquakes on the Guy-Greenbrier fault stopped within months of the shutdown of the injection wells.

Horton (2012) studied ~1,000 earthquakes detected using primarily 4 real time stations in the regional seismic network (Cooperative New Madrid Seismic Network (CNMSN)). The set of

Table 1: Seismic stations shown in Figure 1.

Station	Latitude	Longitude	Elevation	Start date	End date
CH1	35.2666	-92.4035	0.176	6/11/2010	1/11/2012
CH2	35.3341	-92.2982	0.212	6/11/2010	1/12/2012
Q101	35.3323	-92.3482	0.196	8/10/2010	8/10/2011
Q202	35.2550	-92.3031	0.111	9/3/2010	8/28/2011
Q301	35.2676	-92.3689	0.101	1/13/2011	3/11/2011
X102	35.3798	-92.3115	0.206	9/4/2010	3/22/2011
X103	35.1780	-92.3632	0.184	3/23/2011	6/22/2011
X201	35.2926	-92.3623	0.207	8/23/2010	8/11/2011
X301	35.2422	-92.4002	0.112	2/21/2011	10/6/2011
X401	35.3799	-92.3138	0.184	3/22/2011	10/6/2011
WHAR	35.2902	-92.2885	0.184	5/17/2010	Continuing

earthquakes was limited to the larger events in the sequence (~md>2.0). In this study we use 7 local stations (distance <10km) to detect and locate all earthquakes of ml>0.0 between July 7, 2010, and October 20, 2010. We begin with a brief summary of the local geology and hydrogeology followed by a discussion of the methods used including an inversion for an improved 1D velocity model. This is followed by a presentation of results - including the updated catalog, spatial and temporal evolution of earthquakes on the fault plane and frequency-magnitude statistics – and discussion and conclusions.

Geology and hydrogeology

The local study area is part of the Arkoma basin, and it is composed mainly of a thick sequence of Paleozoic sedimentary rocks overlying the Precambrian basement. The top of the basement is approximately 4-5km deep as seen from the stratigraphic cross-section (Figure 2) modified from Caplan (1954). The earthquakes in this study occurred partly in the Paleozoic rocks but mostly in the Precambrian crystalline basement up to a depth of 8km. Regionally the Arkoma basin is bounded by the Ozark Plateau on the north, and the Mississippi embayment to the east (Figure 1 insert). The Precambrian basement shallows to the north of the study area and is exposed in the St. Francois mountains area of the Ozark Plateau in Missouri (Imes and Emmett 1994). To the east, in the Mississippi embayment, the top of the basement is 1-2km deeper than in the study area.

Local UIC wells inject wastewater into the Paleozoic sedimentary rocks (Figure 2). Two major geohydrologic systems occur in the study area (Imes and Emmett, 1994). The upper system consists of several km of alternating sequences of low-permeability shale and low to relatively permeable sandstone, limestone, and coal is called the Western Interior Plains confining system. As a confining system, pockets of permeable zones exist locally but vertical and lateral groundwater flow is impeded because the dominantly low permeable rocks collectively restrict fluid movement (Imes and Emmett, 1994). The Ozark aquifer, essentially overlying the basement, is a thick massive sequence of dolostone, limestone and sandstone formations ranging in age from Late Cambrian to Middle Devonian. Because dolostone is the

Table 2: Class 2 UIC wells shown in Figure 1. Volume and pressure are peak values observed during injection period**.**

| Well	Volume (m^3/month)	Pressure (MPa)	Start Stop	Injection Depth (m)	Aquifer
SRE	62,662	11.8	07/7/10 03/03/11	1821 1969	Springfield/ Ozark
Trammel	54,058	15.8	04/15/09 06/20/11	1982 2009	Springfield
Moore	23,435	20.3	06/15/09 07/27/11	2365 3231	Springfield/ Ozark
Underwood	29,573	5.1	01/15/10 10/15/10	1713 1926	Springfield/ Ozark
Edgmon	19,580	19.6	08/16/10 03/03/11	2379 3344	Ozark
Scroggins	18,629	3.2	04/05/10 NA	678 706	*

* Western Interior Plains confining system

predominant rock type, dissolution of carbonate rocks along fractures and bedding planes is the main source of secondary permeability in the aquifer. The Ozark confining unit is slightly permeable with the relatively thin Chattanooga Shale composed of only 25% shale and 75% sandstone in the study area. The Springfield Plateau aquifer is a sequence of water bearing Mississippian limestone formations known locally as the Boone Formation that forms the upper part of the Ozark Plateau aquifer system. Although the formation has relatively low intrinsic porosity, it remains permeable because of dissolution of limestone along fractures and bedding planes especially in northern Arkansas.

Injection at the SRE well occurs over ~30m in the Springfield Aquifer (Boone Formation) and in the top ~30m of the Ozark aquifer (Hunton Group), with the two aquifers separated by ~14m of the Chattanooga Shale (Figure 2). The injection depth is between 1.84 and 1.92km. At the Edgmon well, injection occurs over the bottom 960m of the Ozark aquifer into the Ordovician age Arbuckle/Knox Group at depths between 2.38 and 3.34km. At the Trammel well, injection is done over ~25m in the Springfield aquifer (Boone Formation) at depths between 2.084km and 2.109km.

In general, most wells in the study area inject into carbonate rocks with relatively low intrinsic porosity, therefore the higher volume wells are sited strategically in areas where secondary permeability from fractures, joints and faults is key to fluid movement in the aquifer. A number of steep basement normal faults have been mapped in the eastern Arkoma basin (Van Arsdale and Schweig, 1990). The faults are continuous from the Precambrian basement upward through the Mississippian terminating at the base of the Pennsylvanian (U in Figure 2). In the study area, the Morrilton fault, the Enders Fault, and the Heber Springs Fault (Figure 1) trend east-northeast sub-parallel to the principal compression axis of the present-day stress field in the mid-continent (Zoback and Zoback, 1991) and are aseismic.

The likely origin of the northeast- southwest (and northwest-southeast) trending basement faults and fractures in the study area is a plate-wide extensional event in the early Cambrian (Burke and Dewey, 1973) that formed the northeast trending Reelfoot rift underlying the Mississippi Embayment. The uplift of the Ozark area also resulted in considerable fracturing and
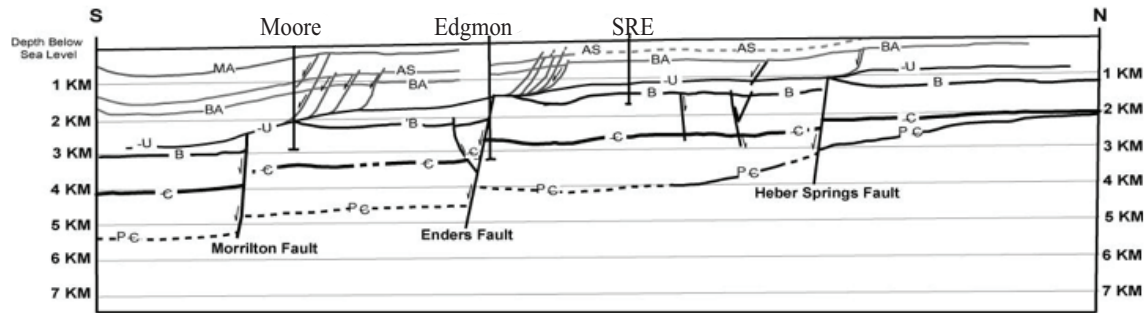
Figure 2: Interpreted geologic cross section modified from Van Arsdale and Schweig (1991) by the Arkansas Geological Survey. MA – Middle Atoka Sandstone; AS - Atoka Sandstone; BA – basal Atoka Sandstone; U - bottom of Pennsylvanian; B - top of the Boone Formation; € - Cambrian; p€ - Precambrian

faulting of the competent carbonate rocks, with widespread and deep erosion releasing stress previously developed in the underlying Mississippian and Ordovician rocks, resulting in faults that approximately parallel the major and minor axes of the uplift (Imes and Emmett, 1994).

Methods

Seismic data

Seismic data for the Guy-Greenbrier swarm was recorded by both permanent and temporary seismic stations. The data from the permanent networks is available from the IRIS/DMC under the standard network codes NM, AG and US. Data from the temporary stations has been archived under the temporary experiment code 7F.

Three seismic stations were within 5km of the Guy-Greenbrier fault prior to the start of injection at the SRE well on 7 July 2010 (see Figure 1 and Table 1). WHAR is a permanent AG network station deployed in February 2010. It is a high quality broadband station. CH1 and CH2 were shallow borehole stations deployed in June of 2010 by Chesapeake Energy, INC. The data from these stations was not available for real-time processing by the CNMSN, and we use it for the first time in this study.

Four other temporary seismic stations were deployed within 5km of the Guy-Greenbrier fault with the intention of recording induced seismicity at the start of injection at the SRE (7 July 2010) and Edgmon (18 August 2010) wells. Two of these (X102 and X201) were real-time broadband stations were processed by the CNMSN. Ten seismic stations were ultimately located within 5km of the Guy-Greenbrier fault.

Improved 1D velocity model

In order to facilitate long-term high quality monitoring of seismicity in this region, we developed an improved 1-D velocity model that takes into consideration the varying velocity structure within the region. The combined monitoring network recorded thousands of events during the period of 2010-2011. The recording distance ranged from 2km to more than 250km from the epicenter. We used the dataset of events used by Horton (2012) for relocation using

hypoDD. In this study, we used the original arrival times and locations recorded in the Center for Earthquake Research and Information (CERI) catalog. The CERI catalog has all arrival time data processed manually and the quality of each arrival time is usually estimated by assigning observational weights that correspond to a given uncertainty in picking the arrival time. For the purpose of robustness, we selected a set of 590 earthquakes out of 1300 with a minimum of six P and S-phase observations and azimuth gaps <180 °. We chose Station WHAR (in Figure 1) as the reference station, since it is the most centrally located within area of interest and is one of the stations that recorded the highest number of events throughout the recording period. We assigned phases recorded by stations in Table 1 the highest weights.

We computed a minimum 1D model using the routine VELEST (version 3.1) (Kissling *et al.* 1995). The algorithm forward calculates travel times using ray tracing (Lee and Stewart 1981; Thurber 1983) while simultaneously inverting the P and S to solve for the combination of velocity model, station corrections, and hypocenter parameters that minimize data misfit. We jointly inverted for the earthquake hypocenter and 1D velocity model using 1D model based on Chiu *et al*. (1984) for the Arkoma basin and a model used by CERI and by Horton (2012) as the initial models (Figure 3). We used the local crustal stratigraphy derived from seismic reflection profiles provided by the ARCO Oil and Gas Company (Chiu *et al*. 1984) to define the velocity layers. The final minimum 1-D model was obtained where simultaneous inversions converged to the minimum root mean square (RMS) residual. The stability test for the hypocenter locations (Figure S1) and the improved 1D model (Figure S2) can be found in the electronic supplement. Figure 3 compares the initial models with the final model presented in Table 3.

The improved 1D model, with station corrections (Figure S3 and S4, available in the electronic supplement to this article), reduces the average RMS-error for the 590 events from 0.207 sec to 0.045 sec. This is an overall reduction in RMS of more than 4 times with respect to the average RMS value for the same data set achieved by using original CERI location model. Figure S5 and S6 (available in the electronic supplement to this article) show that the improved 1D model earthquake hypocenters are almost similar to hypocenters achieved through HypoDD relocation.

Updating the catalog

The central area of interest, the Guy-Greenbrier fault, had at least six broadband stations within a 10km radius that were continuously recording at any given time (Table 1). We used mainly these stations for analysis since their proximity provided good signals especially for the small sized earthquakes. Using the Antelope software package, we optimized the event detector using STA/LTA ratios greater than 2 for a time window of 0.5/4 sec and frequencies between 1-16 Hz. We ran an automatic detection and event association of the arrival times and then manually picked P and S arrival times while discarding any false picks to avoid introduction of errors in location. We used a minimum of five stations to locate the earthquakes using the GENeric LOCation algorithm (Pavlis *et al*. 2004) using the new minimum 1D model.

A total of 17,395 events were located using ~86,714 P wave and ~80,163 S wave arrivals for the period between 7 July 2010 and 20 October 2010, which is ~100 times the number of events in the regional catalog for the same time period. The mean number of phases used for location was 8 with 94% of the events located using more than 6 phases. We calculated the local magnitude using a station correction of 1.4 for distance <5km and 1.5 for 5km>distance<10km. Figure 4 shows the locations of the earthquakes in the updated catalog that are further grouped according to characteristics of different sections of the fault.
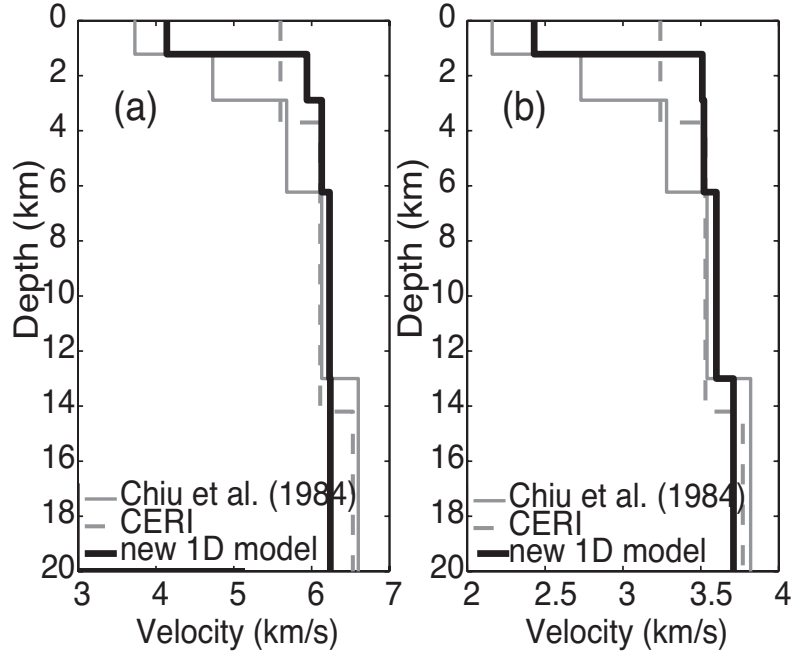
Figure 3: Initial and final velocity models for (a) P-wave, (b) S-wave

Table 3: Updated Central Arkansas 1D Velocity Model

Depth (km)	P-wave (km/sec)	S-wave (km/sec)	V_P/V_S
0	4.14	2.43	1.704
1.22	5.94	3.51	1.692
2.89	6.13	3.52	1.741
6.23	6.23	3.60	1.731
13.00	6.24	3.71	1.682
40.00	8.15	4.68	1.741

Results

Analysis of the continuous seismic waveforms has revealed many more seismic events than the number recorded in the CNMSN catalog. Most of these events are of magnitude M<2 and may be insignificant in monitoring regional seismicity for seismic hazard analysis. However, microseismic events due to pore-pressure perturbation can be used to delineate weak regions within the crust that have the potential of failure under favorable conditions. The updated catalog

presents a more robust dataset to analyze the properties of the illuminated faults and a platform for better understanding of the initiation and migration of seismicity along the fault.

By locating small magnitude events, we discover a new fault area composed of ~750 microseismic events that occurs ~2km west of the Guy-Greenbrier fault. This is a swarm of events that happen (i.e. 95% of the earthquakes) within four days starting at 10/04/2010. The events in this cluster are of magnitude lower than ml=1.5, and therefore the absence of moderate to large size earthquakes places the cluster below the regional catalog threshold. The timing of the western cluster coincides with hydraulic fracturing activity in a nearby well and the seismicity is located directly beneath the lateral horizontal well. The timing and location provide a strong indication that the earthquakes are due to the hydraulic fracturing process.

The Guy-Greenbrier fault system

The Guy-Greenbrier earthquake sequence illuminated the previously unknown ~13km long vertical fault system (Figure 1) from north to south during the fall of 2010 and spring of 2011 (Horton, 2012). In this study details of the ~ 7.5km long northern section (Figure 4) of the fault system are revealed by the increased resolution provided by the new earthquake catalog. The northern fault section can be described as a system of 3 joined fault sections based on the concentration of hypocenters and the size distribution of events in each section. At the northern end of the fault is the ~1.5km long northern section (N) that is elongated in an ENE direction. This section appears to dip at high angle to the north. In the middle is the ~2.0km long central section (C) that strikes N30°E. The ~4km long southern (S) section also strikes N30°E but plunges at ~5° to the south.

Seismicity migration over time

Seismicity on the Guy-Greenbrier fault has a unique occurrence pattern. The beginning of injection at the SRE well on July 7, 2010, was followed by scattered events with no particular spatial-temporal pattern within a radius of ~6km from the well. Four of these small scattered earthquakes (ml < 2.0) happened to occur along the S section of the Guy-Greenbrier fault on August 6, 2010.

The first consistent swarm of earthquakes on the Guy-Greenbrier fault began around August 29, 2010, close to the SRE well at ~3km depth on the north section (Figure 5a). The seismicity started in the Paleozoic sedimentary rocks but by September 8, 2010, had spread into the Precambrian crystalline basement to depths around 4.5km. In the NS cross section (Figure 5b) the earthquakes are distributed in two distinct trends both dipping north at high angle. At that time, seismicity decreased significantly in the north section until October 14 when a new and stronger phase of seismic activity began (Figure 5g, Figure 6a). The renewed seismic activity occurred in the same distinct bands as the previous swarm. The first earthquake with ml > 2.0 (ml=2.0) in this section occurred on October 17, 2010 along the basement boundary (Figure 7).

Low-level seismic activity began in the central section around September 9, 2010, (Figure 5b-d and Figure 6b) with higher rates of seismic activity on October 2-3, 2010. The first m>2.0 earthquake (ml=2.96) occurred in the section on October 1, 2010. This seismicity occurred primarily in the Paleozoic section ~2km SW of the SRE well, and extended somewhat into the Precambrian basement (Figure 5d). A short lull in seismic activity followed with seismicity rates picking up again on October 14, 2010. The central section strikes N30°E with no plunge.

The first four earthquakes (ml< 2.0) to occur along the southern section of the fault occurred on August 6, 2010, 30 days after the initiation of injection at the SRE well (~6.0km
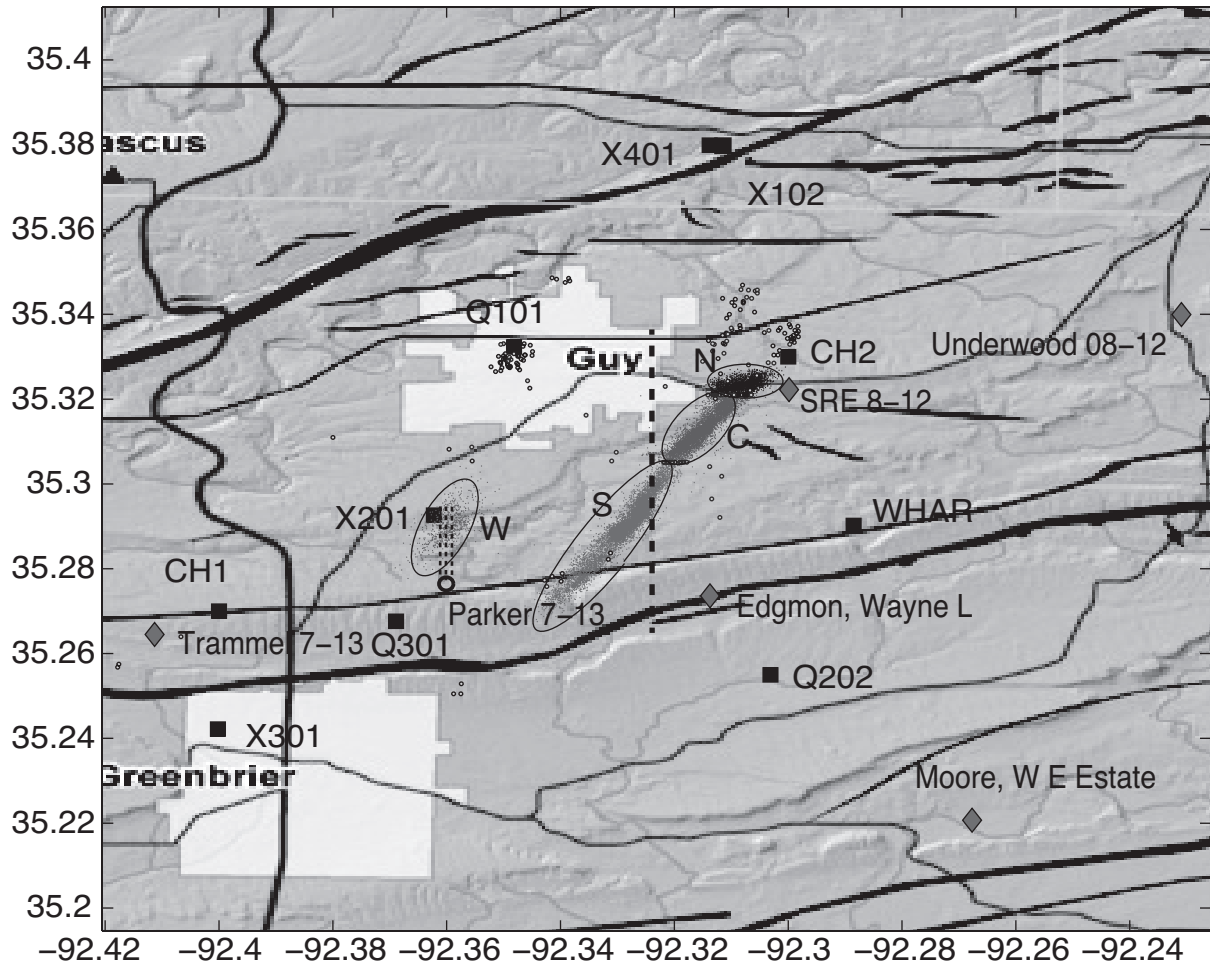
Figure 4: Seismic stations (black square), UIC wells (grey diamond), earthquakes (grey) between 07/07/10 and 10/20/10. Earthquakes were located using dbgenloc algorithm (Pavlis *et al*. 2004) and with the improved velocity model. Earthquakes are grouped into N-northern section, C-central section, S-southern section and W-western swarm. The dashed line is the line of the cross-section in Figure 5 and Figure 6.

distance) and 10 days before the start of injection (August 16, 2010) at the Edgmon well (2.5km distance). These events occur ~0.3km west of a natural gas production well that was hydraulically fractured at this time and completed on August 6, 2010.

Low levels of seismic activity on September 14, 2010, mark the beginning of continuous seismicity in the southern section (Figure 4 and Figure 5b). These earthquakes occurred at ~3.5km southwest of the SRE well at ~5km depth within the Precambrian basement. The seismicity rate remained low as this earthquake activity spread southward to cover an area of ~1.5km radius from the point of initiation within ~28 days (orange in Figure 5f) by October 11, 2010. The first earthquake on the Guy-Greenbrier fault with ml>2.0 (ml=2.5) occurred on September 23, 2010, about 4km southwest of the SRE well and 2.3 km northwest of the Edgmon well. This event marked the startup time and location inferred by Horton (2012) from earthquakes located by the CNMSN regional network. The seismicity rate started to rise to moderate levels in the southern section around October 9, 2010 with the first occurrence of ml>
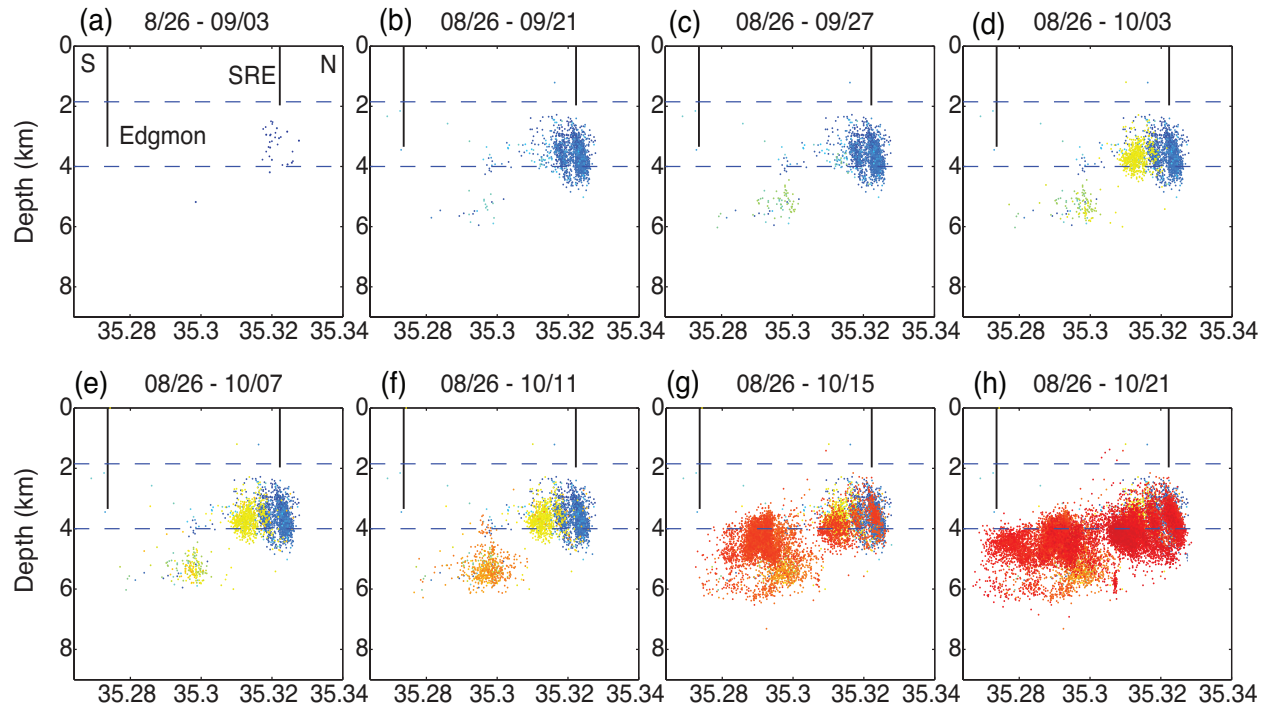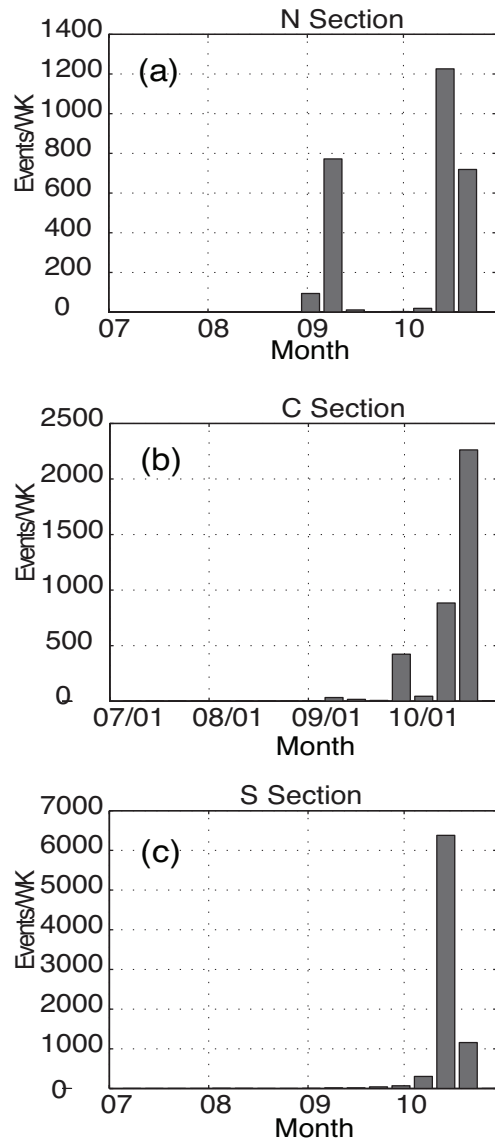
Figure 5: N-S cross-sections showing earthquake hypocenters, the location of SRE well and Edgmon well. The color transitions in time from 08/26/2010 (blue) to 10/21/2010 (red). The dashed lines denotes the top of the Boone Formation at ~1.85km and top of the Precambrian basement at ~4km.

3.0 (ml=3.5 and ml=3.2) earthquakes on that date. The seismicity rate jumped to very high levels (>1000 events per day) on October 12, 2010 following the occurrence the first Mw=4.0 earthquake on October 11, 2010.

Beginning October 11, 2010, another swarm began within the Precambrian basement right above the initiation point of the southern section seismicity, and grew southward to illuminate a ~5km section of the fault (Figure 5h) within 7days. In the area near the initiation point, the swarm rose above the top of the Precambrian crystalline basement into the Paleozoic sedimentary rocks. At the same time, precisely beginning October 13, 2010, in the northern section, seismicity started to re-occur over the entire area that had been earlier illuminated (red in Figure 5g). This time the swarm seemed to propagate from north to south in time without discontinuing at the start point. This phenomenon also characterized the southern section. Later on, the seismicity grew to connect the two sections into one ~N30°E trending fault ~8km in length.

The northern section has 70% of the events located within the Arbuckle Group while the central section has most of the seismicity occurring between approximately 2.5km and 5km depth with a seemingly even event distribution between the Arbuckle Group and the Precambrian basement. In the southern section, ~90% of the seismicity is confined within the basement.

Figure 7 shows that event size distribution with depth varies in each of the three sections although in general most of the small events (ml<1) are shallow (depth <5km) while the largest events (ml > 4) are deep (depth > 5.5km). During this time period, the northern section is

Figure 6: Histograms showing earthquakes per week in each section. In general seismicity starts in the northern sections and progress to the south.

characterized by small magnitude events (i.e. ml<3) where the larger events occur well within the swarm of small events especially with respect to depth. Earthquakes in the northern section are located primarily in the Arbuckle Group. Within this section, there seems to be two patches, one with fewer and smaller events to the south and the other with most of the events and containing the largest magnitudes (with respect to this group) to the north.

The central section has both the number of earthquakes and magnitudes scattered almost evenly between the Arbuckle Group and the basement (Figure 7). The larger events in this section seem to align along the vertical edge with the northern section. The southern section has the largest earthquakes (i.e. ml>4) in the updated catalog, and the larger events are the deepest events. Magnitudes reduce towards the top of the fault.
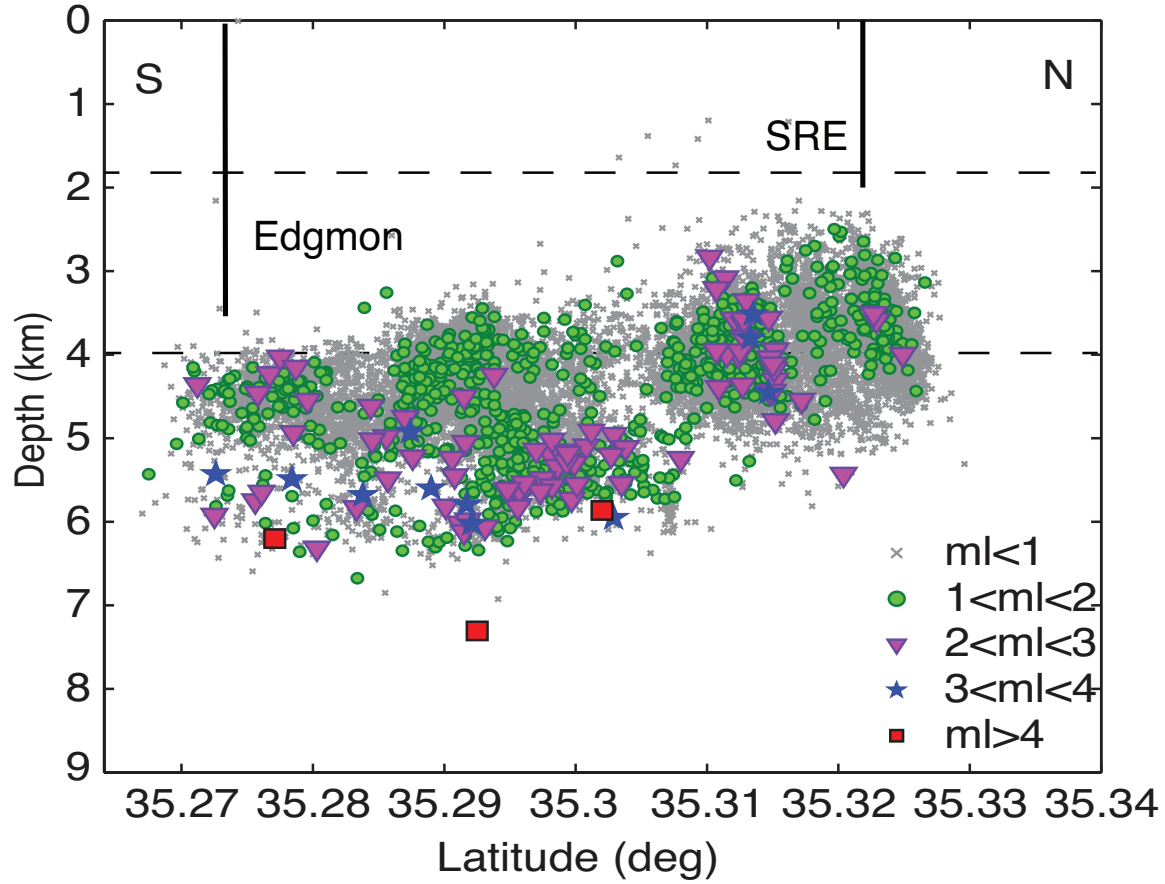
Figure 7: N-S cross-section showing earthquake hypocenters, the location of SRE well and the Edgmon well. Earthquakes are grouped for different ranges of magnitudes. The dashed lines denotes the top of the Boone Formation at ~1.85km and top of the Precambrian basement at ~4km.

Catalog completeness

The magnitude–frequency distribution during the Guy-Greenbrier sequence can be evaluated using the Gutenberg–Richter relationship, $\log N = a - bM$, where N is the number of events with magnitudes equal to or above M, and a and b are constants (Ishimoto and Iida, 1939; Gutenberg and Richter, 1944). The a parameter describes the productivity of a seismogenic zone while b is the slope of the frequency–magnitude distribution describing the size distribution of earthquakes (Wiemer and Wyss, 2002). The minimum magnitude of completeness, above which all earthquakes can be detected, is estimated to be ml~0 for the analyzed earthquakes for the Guy-Greenbrier sequence (Figure 8).

We have evaluated the b-value for the entire catalog, then separately for each of the three sesections on the fault system, and for the cluster of events located to the west. The entire catalog has a b-value of 1.1 with earthquake size ranging between 0<ml<4.1. The b-values for the north, central and southern sections are 1.45, 1.1 and 1.0, respectively. Having noticed the imbalanced
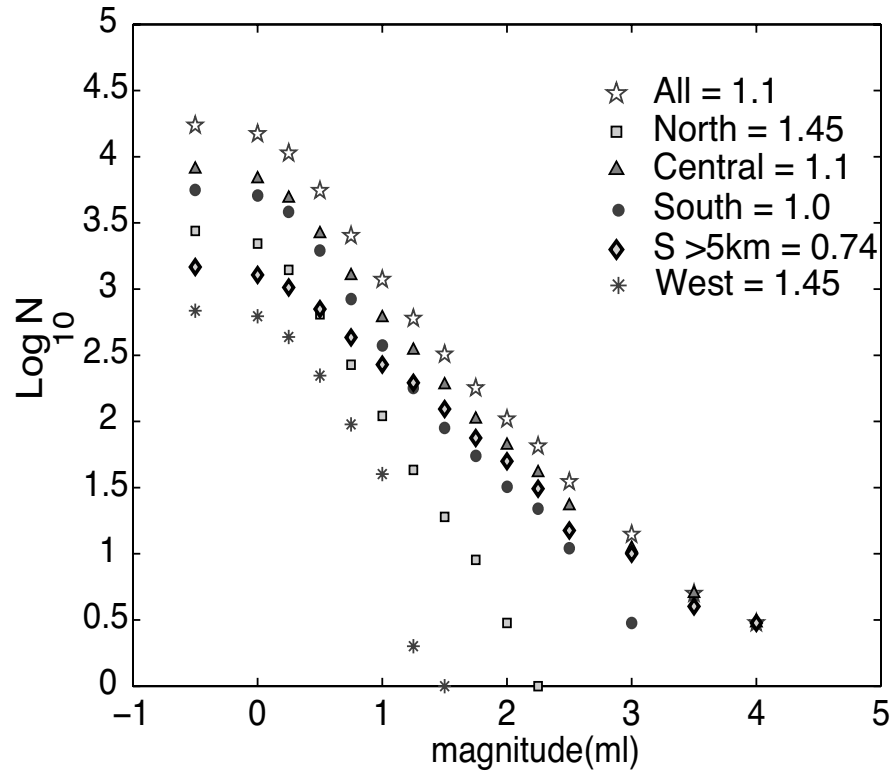
Figure 8: The Gutenberg-Richter magnitude-frequency plot for different grouping of micro-earthquakes. The legend shows the b-value for: All- all the events located; North- events in the northern section; Central– events in the central section; South- events in the southern section; S>5km- events in the southern section of depth>5km; West- swarm of events west of the main fault.

distribution of event magnitude with depth especially for the relatively flat bottom of the southern section of the fault, we have further evaluated the b-value for events below 5km depth. The b-value for these events that were not accompanied by smaller events was 0.78. The small earthquakes located west of the Guy-Greenbrier fault have a b-value 1.45 and ml=1.5 as the largest magnitude.

Discussion and conclusion

The interpretation of the migration pattern of seismicity in space and time is highly dependent on the minimum size of the events available. Horton (2012) suggested that the Guy-Greenbrier earthquake sequence started with a swarm of ml>2.0 earthquakes (the real time low magnitude location threshold) on ~September 23, 2010, ~4km southwest of the SRE well based on earthquakes detected and located by the CNMSN. However, this study clearly shows the first consistent swarm of earthquakes (ml<1.7) on the Guy-Greenbrier fault began on August 29, 2010, ~660meters west of the SRE well at ~3km depth.

We found that earthquakes are not distributed uniformly along the Guy-Greenbrier fault but can be clustered into three sections with somewhat different earthquake behavior. These sections coincide with structural features of the Fayetteville Shale. An overlay of the seismicity on a contour map of the top of the Fayetteville Shale (Figure 9) shows some correlating features
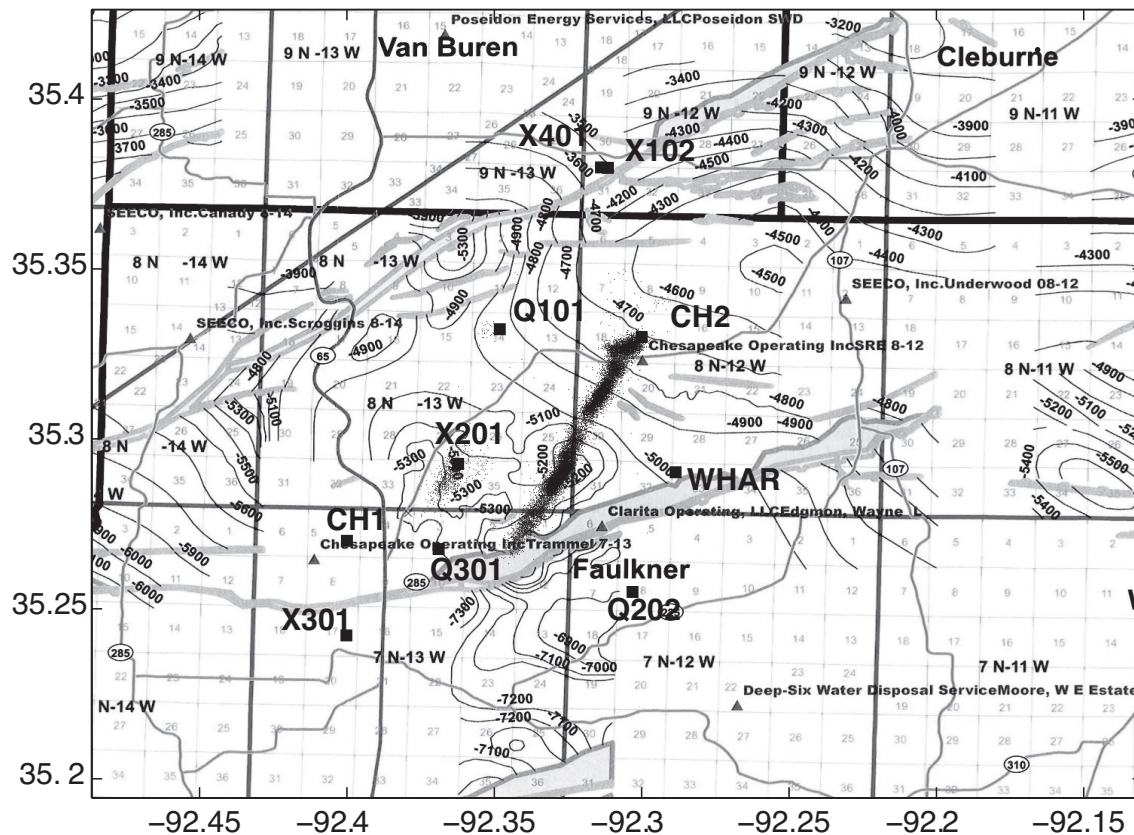
Figure 9: Depth contour map of top of Fayetteville shale and the location of seismicity (black dots). The bold grey lines are basement faults. Black filled squares are seismic stations and black filled triangles are wastewater injection wells. The gridding on the map follows Public Land Survey System with the larger squares being townships while the smaller squares are sections. (Map courtesy of Arkansas Geological Survey & Gas Commission).

that may explain the nature of the fault system. The gridding on the map follows the Public Land Survey System with the larger squares being townships while the smaller squares are sections. Between the Heber Springs fault zone to the north and the Enders fault zone to the south is a large structural high (dome) centered at Sections 2, 3, 10 and 11 in T8N, R12W. The Guy-Greenbrier Fault is located on the SW flank of this dome where the structure dips to the southwest from -4,700 ft at the northeast end to -5,300 ft just north of the Enders fault zone. The -5,000 ft contour that marks the edge of the dome coincides with the joining of the central and southern sections. The SW plunging southern section is coincident with the change in slope of the Fayetteville Shale SW of the -5000 ft contour.

The ENE elongation direction of the northern section is unfavorably close to the N65°E regional principal stress orientation (Zoback and Zoback, 1991). Therefore, we do not expect earthquakes on ENE trending faults. Rather, we expect strike-slip earthquakes on small sub-parallel faults striking NE that fill-in this area. The unfavorable orientation may explain the deficiency of higher magnitude events during this time period given the proximity of the fault section to the injection well. This is supported by the focal mechanism of the largest event (Mw3.9) in the northern section that has a vertical nodal plane trending N15°E. This earthquake occurred on November 20, 2010 at 4.5km depth. The orientation and positioning of the northern

section seems to impede further development of the Guy-Greenbrier fault to the north. The orientation of the northern section may be part of the dome's fracture system mentioned above. By analyzing the timing, location and migration of the ml< 2.0 events, we are now able to attribute seismic activity in the northern section completely to the SRE well based on proximity and timing. However, activity in the relatively central and southern sections seem to occur at separate time periods and not concurrently until beginning October 15, 2010 and therefore it is not clear how the two wells contribute to induce seismicity in the sections by only observing spatiotemporal occurrence of the seismicity.

The overall dataset's b-value is close to 1.0, the b-value of naturally occurring earthquakes (Gutenberg and Richter, 1944) suggesting the earthquakes occur in an area where faults and fractures are critically stressed (Zoback and Townend, 2001). The overall b-value indicates a significant large number of small events in the dataset. However, the event size distribution along the fault is not uniform as seen from the variation of b-value for different groups of events. In general larger events tend to occur at the bottom of the fault and smaller events tend to concentrate near the top. This variation in earthquake size with depth is also accompanied by an increasing b-value with depth especially in the southern section. Warpinski *et al.* (2012) found a trend of increasing magnitude with increasing depth in hydraulic fracturing and attribute this trend to the prevailing stress gradient.

Data and resources for Part 1

Seismograms used in this study were collected primarily as part of an unfunded induced earthquake experiment conducted by CERI and the AGS using the AG network, portable instruments from CERI and 2 USGS temporary stations. Chesapeake Energy also provided data from two local seismic stations. All seismic data have been archived and can be obtained from the IRIS Data Management Center at www.iris.edu (last accessed August 2015).

Part 2: *Numerical model of pore-pressure diffusion associated with the initiation of the 2010–2011 Guy–Greenbrier, Arkansas earthquakes.*

Paul O. Ogwari and Stephen P. Horton

Introduction

Fluid waste disposal wells are used for injecting contaminated fluids into highly saline porous aquifers bounded by nearly impermeable formations in the deep subsurface. The main safety concern with these waste disposal wells has always been the possible flow of waste fluids out of the targeted aquifers into shallow freshwater aquifers contaminating drinking water, and they must meet Underground Injection Control (UIC) regulations provided by the Environmental Protection Agency (U.S. Environmental Protection Agency 1985; Hatzenbuhler & Centner 2012). Recently, deep injection waste disposal has raised concern over seismic hazard following the increase, up to six times in the last decade or so (Ellsworth *et al*. 2012), of seismicity associated with deep wastewater injection (Frohlich 2012), especially of moderate magnitude.

Between September 2010 and July 2011, a swarm of small- to moderate-size (M ≤ 4.7) earthquakes illuminated the previously undetected Guy–Greenbrier fault in Arkansas (Horton 2012) requiring shut-in of four UIC wells within 10 km radius of the seismicity. After the shut-in, the seismicity rate dropped significantly, and there is no current seismicity associated with the Guy–Greenbrier fault. Although a clear spatial and temporal connection is evident between the fluid injection and the earthquakes, the pressure migration from the wells to the fault is not thoroughly understood. In a separate paper, we analyzed the first three and half months of seismicity following the start of injection at the SRE well (July 7, 2010) to produce a catalog of over 17 000 earthquakes with magnitude completeness of ml = 0.2 (Fig. 1) and found the precise timing and distribution of seismicity (Ogwari *et al*. 2016). We detected and located the earthquakes using the Antelope software package. The detections were optimized using STA/LTA ratios >2 for a time window of 0.5/4 sec and frequencies between 1 and 16 Hz. We ran the automatic detection and event association of the arrival times and then manually picked P and S arrival times while discarding any false picks to avoid introduction of errors in location. Finally, we located the earthquakes using the GENeric LOCation algorithm (Pavlis *et al*. 2004) with a new 1D velocity model. In this study, we model pore-pressure diffusion caused by pressurized waste-fluid injection at two nearby wells and then compare the buildup of pressure with the observed initiation and migration of earthquakes.

The study of induced seismicity due to wastewater injection dates back to 1960–1970s (e.g., Healy *et al*. 1968; Raleigh *et al*. 1976). These studies were prompted by a sequence of earthquakes occurring near Denver, Colorado between 1962 and 1967, with the largest event being a M5.2, following hazardous waste injection at the Rocky Mountain Arsenal between 1962 and 1966 (Healy *et al*. 1968; Hsieh & Bredehoeft 1981). Raleigh *et al*. (1976) carried out a series of controlled experiments at the Rangely oil field in northwestern Colorado, where variable rates and volumes of injection indicated the rates of seismicity were modulated by the injection parameters. A study by Keranen *et al*. (2014), following the 2008 Jones, Oklahoma sequences, suggests that much of the activity may be associated with a few very high volume injection wells
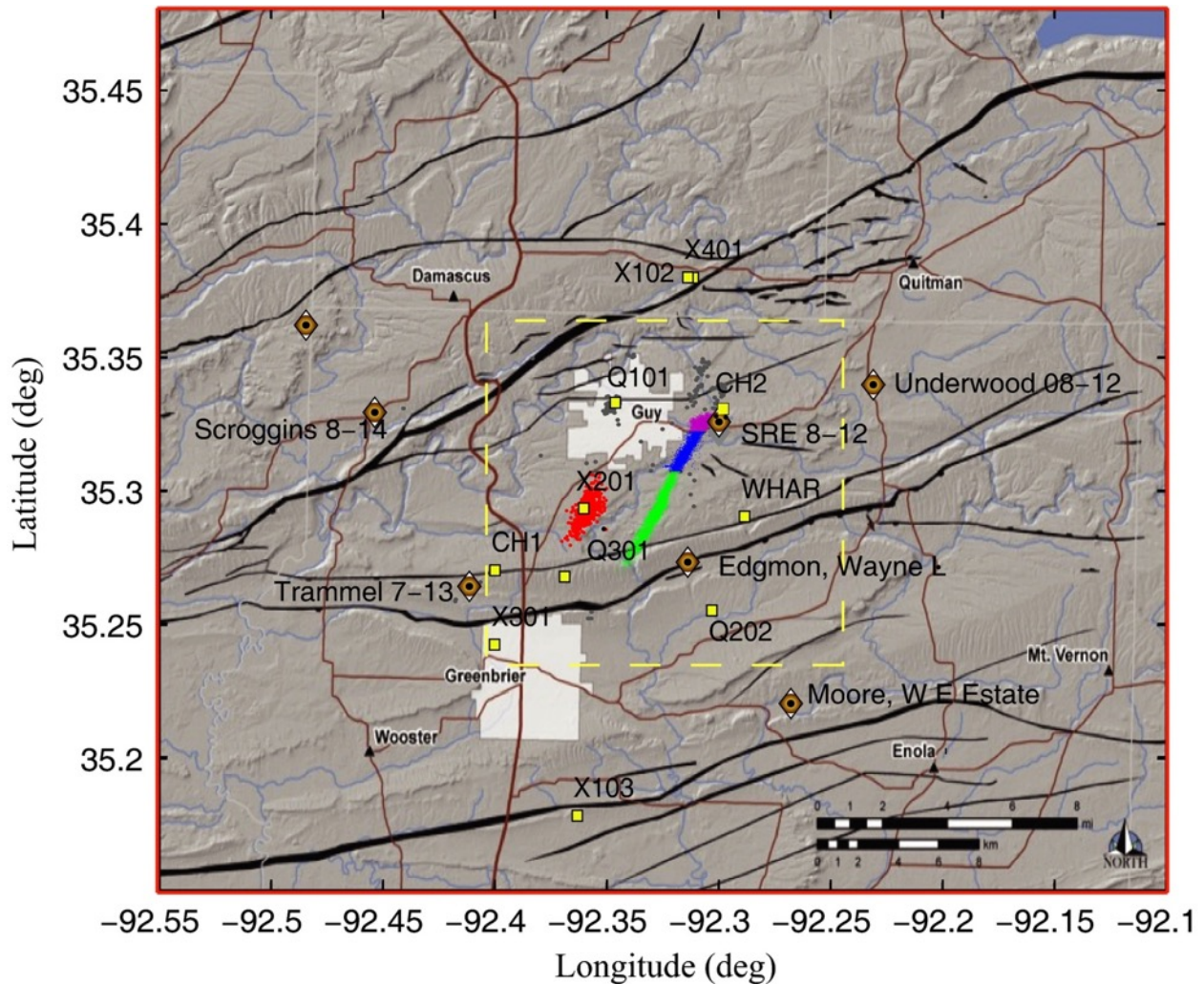
Figure 1: Earthquakes (gray and dots) located in Guy–Greenbrier between July 07, 2010 and October 20, 2010, Seismic stations (yellow squares) and UIC wells (brown/black diamonds). Earthquakes are grouped into N, northern section (pink); C, central section (blue); S, southern section (green); and W, western swarm (red) based on their spatiotemporal occurrence. The seismicity in gray, as well as the western swarm, has been associated with hydraulic fracturing activities and has not been considered in the analysis. The red solid line indicates the edge of the modeled area while the yellow dashed line demarcates the area presented in the model results.

that are propagating pore-pressure pulses up to tens of kilometers from the wells to induce seismicity. A damaging 2011 M*w* 5.7 earthquake also occurred near Prague, Oklahoma, that may be triggered by fluid injection. The Prague, Oklahoma, events occurred nearly 20 years after the initiation of injection, and about 5 years following the most substantial increase in wellhead pressure (Keranen *et al*. 2013). The 2010–2011 Guy–Greenbrier sequence occurred within months of the start of injection, providing a unique dataset to analyze the nature of pressure diffusion and distribution within the aquifers and aquitards.

To induce earthquakes by increased pore pressure requires more than changing the elastic stresses especially at distances of tens of kilometers. As the UIC regulations require that the

injection pressures in the disposal wells never reach the fracture limit of the overlying aquitard (U.S. Environmental Protection Agency 1985), the energy to cause slip on the fault cannot be directly from the injection fluid. Faults with favorable orientation with respect to the regional stress field that are near failure are necessary for a minimal change in pore pressure to trigger earthquakes (Nicholson & Wesson 1990; Barton *et al*. 1995; Townend & Zoback 2000; Zoback & Townend 2001). Various studies have reported a range of triggering pressures. For the Rocky Mountain Arsenal case, fluid pressure changes of 3.2 MPa were deemed needed to induce earthquakes (Hsieh & Bredehoeft 1981) at distances <10 km from the well. In Oklahoma, Keranen *et al*. (2014) have suggested a critical threshold of approximately 0.07 MPa pore-pressure increase triggered earthquakes to distances as far as approximately 35 km from the wells. Rothert & Shapiro (2007) found an increased pore pressure between 0.001 and 1 MPa was required to trigger earthquakes during the Hot Dry Rock experiment in Soultz, France. In this study, we will estimate the threshold pore-pressure increase necessary to induce seismicity in the Arbuckle Group of the Ozark aquifer and in the deeper crystalline basement fault.

We create a 3D hydrogeological model of the Arkoma basin. We estimate the hydrogeologic properties of the local aquifers using observed well pressure data. The injection area is intersected by major faults that cut through the Ozark aquifer into the basement (Fig. 1). We constrain the hydrogeologic properties of the local faults from the rate of seismicity migration following injection. We incorporate as many of these faults into the model as possible because they may act as conduits for pressure diffusion. We calculate the change in pore pressure with time and distance in the 3D model due to the observed daily injection volumes. We then compare the seismicity pattern to the pore-pressure diffusion field.

Hydrogeology

The study area is located on the eastern side of the Arkoma basin. The basin in the area of study has two major hydrogeological systems (Imes & Emmett 1994), the Western Interior Plains confining system (area above B in Fig. 2) and the Ozark aquifer (area between B and p€). Separating the two are the Springfield Plateau aquifer and the Ozark confining unit, although they are not indicated on the cross-section. The upper several kilometers of stratigraphy is the Pennsylvanian age Western Interior Plains confining system consisting of alternating sequences of shale and sandstone, limestone, and coal. The dominating low permeability rocks restrict vertical and lateral groundwater flow although permeable zones exist locally.

Below the Western Interior Plains confining system is the Mississippian age Springfield Plateau aquifer consisting of limestone (locally known as the Boone Formation) with relatively low intrinsic porosity, and whose permeability has been enhanced by dissolution of limestone along fractures and bedding planes (Imes & Emmett 1994). The Springfield Plateau aquifer is underlain by the Devonian age Ozark confining unit, a unit primarily made of Chattanooga Shale. In the study area, the confining unit is relatively thin consisting of approximately ten meters of sandstone and about three meters of shale (S. Ausbrooks, personal communication). Below the Ozark confining unit is the Ozark aquifer, the thickest aquifer in the study area. The Ozark aquifer is of Ordovician and Silurian age and can be subdivided into Hunton, Viola, Simpson, and Arbuckle groups in that order from the top. The Ozark aquifer is composed of dolostone (mostly in the Arbuckle) as the dominant rock type together with some limestone (in the Hunton and Viola) and sandstone formations (partly in the Simpson). The dolostone has relatively low intrinsic porosity (approximately 4–6%), but porosity is enhanced in fractured and faulted areas, and these areas are likely to have the greatest permeability.
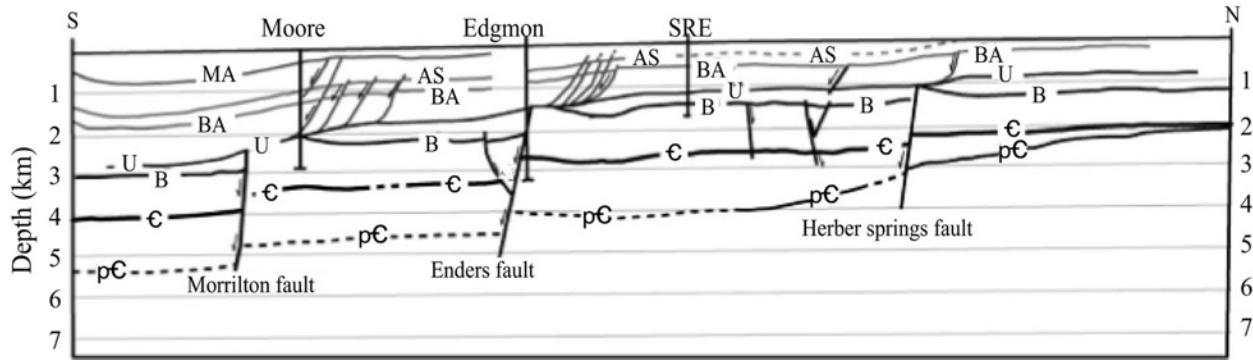
Figure 2: Interpreted geologic cross-section modified from Van Arsdale & Schweig (1990) by the Arkansas Geological Society (Horton 2012). MA—middle Atoka sandstone; AS—Atoka sandstone; BA—basal Atoka sandstone; U—bottom of Pennsylvanian; B—top of the Boone Formation; €—Cambrian; p€—Precambrian.

In the study area, there is a notable absence of the St. Francois confining unit, a clastic and carbonate rock formation with variable shale content, and the St. Francois aquifer consisting of a moderately permeable Bonneterre Dolomite and the Lamotte sandstone formation (Caplan 1960). This means there is no impermeable unit to stop fluid migration from the Ozark aquifer into the Precambrian basement faults. The basement is composed of generally low permeability crystalline rock and generally acts as a confining unit except where faults and fractures provide conduits for fluid movement.

Micro-Earthquake Sequence

Seismicity on the Guy–Greenbrier fault occurs in three distinct patches based on the concentration and timing of the hypocenters (Ogwari *et al.* 2016). The seismicity is characterized by preceding few scattered events that are followed by swarms of events in the three sections of the fault. The first seismic swarm sequence begins under the SRE well after about 58 days (August 29, 2010) of injection at the well. The swarm initiates at approximately 3 km depth (Fig. 3A) and spreads deeper to approximately 4.5 km depth. The initial seismicity illuminates a steeply north dipping fault section (northern section). Seismicity continues to occur in the following days and migrates south.

On day 82 after the start of injection at the SRE well and approximately 41 days after the start of injection at the Edgmon well, another swarm of seismicity started approximately 3.5 km SW of the SRE well at approximately 5 km depth within the Precambrian crystalline basement to mark the beginning of seismicity in the southern section (Fig. 3B). This seismicity spreads southward to cover an area of approximately 1.5 km radius, from the point of initiation, and continued to occur for days at a low rate. During the same period, after around 86 days of injection at the SRE well, seismic activity in the central section started to migrate southward primarily within the Arbuckle Group in the central section and at 5–6 km depth in the basement in the southern section (Fig. 3C). The rate of seismicity was higher than in the previous episode and was sustained for approximately 5 days before decaying.

After the sustained episode of activity in the central section, about 96 days of the injection period, another seismicity swarm began within the top 1 km of Precambrian crystalline basement and the bottom of the Arbuckle Group right above the initiation point of southern
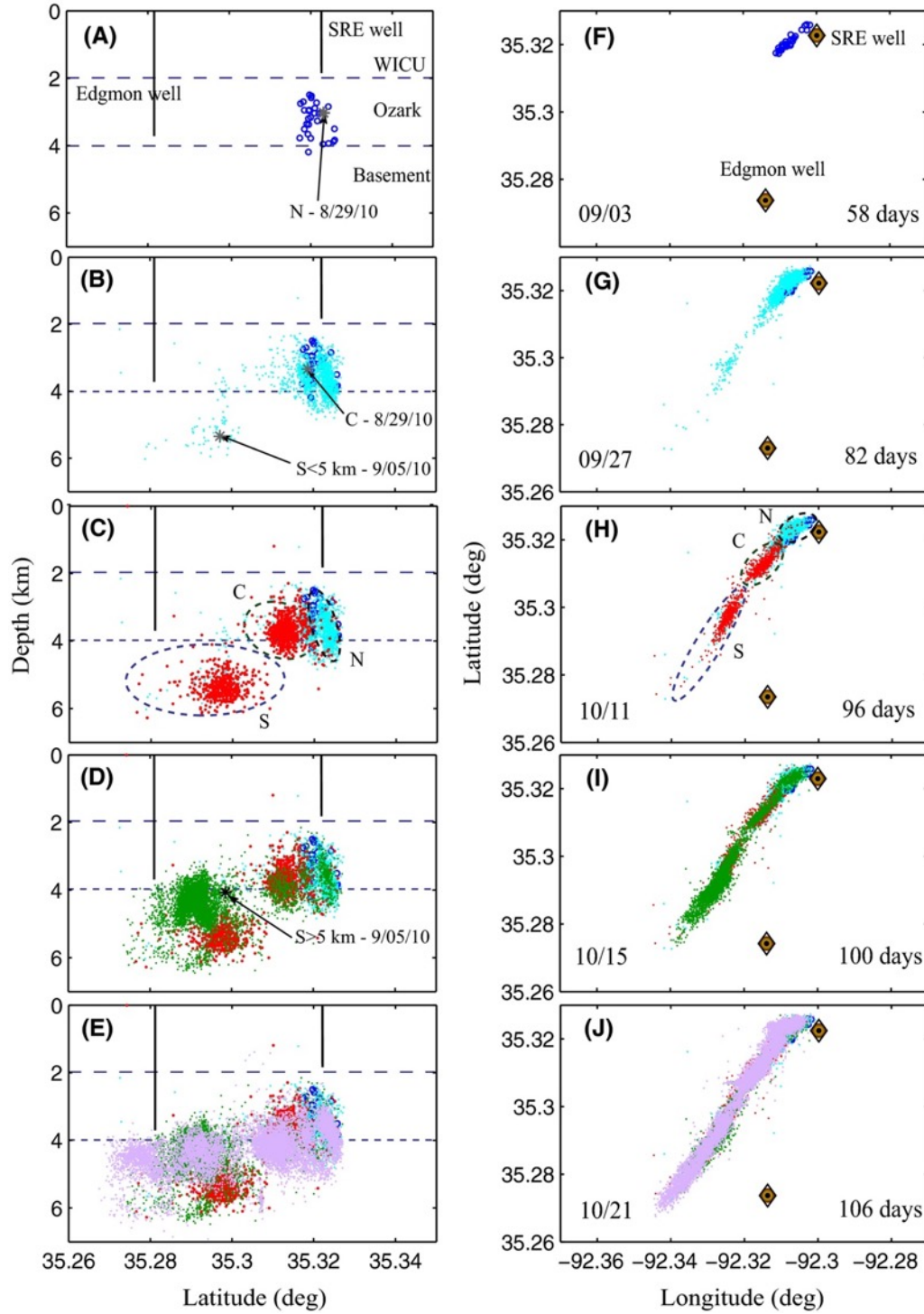
Figure 3: Vertical cross-sections (left) and horizontal plane view (right) of earthquake hypocenters (dots and circles) located on the Guy–Greenbrier fault color-coded for the time interval of the plots. The plots correspond to (A, F) 58 days, (B, G) 82 days, (C, H) 96 days, (D, I) 100 days, and (E, J) 106 days of injection with respect to the SRE well. The date-marked events (asterisk) indicate the first event of each of the N, C, and S grouping of earthquakes. The dashed horizontal lines indicate the confines of the Ozark aquifer.

section seismicity (Fig. 3D). The swarm grew southward to illuminate a approximately 6-km section of the fault within 9 days. During this period, seismicity started to re-occur at a higher rate on the northern and central sections, covering the entire area that had earlier been illuminated. The swarm seemed to propagate from north to south as a function of time with sustained activity at the starting point. This is a phenomenon that also characterized the southern section. Later on, the seismicity grew to connect the three sections into one approximately N30E fault of approximately 7.4 km in length (Fig. 3E). In summary, the seismicity on the Guy–Greenbrier fault started in the Paleozoic sedimentary rocks and spread into the top of Precambrian crystalline basement. We analyze significant periods to understand pore-pressure diffusion in the area of study.

Methodology

We start by populating the model grid with hydraulic parameters needed in the modeling process of pore-pressure diffusion. The MODFLOW program requires permeability, storativity, and porosity of the formations and the faults. We apply different methods to extract the model parameters depending on the available information.

Transport Equations

MODFLOW-2005, a modular finite-difference code developed at the USGS, implements the partial-differential equation of ground-water flow as (Harbaugh, 2005)

$$\frac{\partial}{\partial x}\left\{K_{xx}\frac{\partial h}{\partial x}\right\} + \frac{\partial}{\partial y}\left\{K_{yy}\frac{\partial h}{\partial y}\right\} + \frac{\partial}{\partial z}\left\{K_{zz}\frac{\partial h}{\partial z}\right\} = S_s\frac{\partial h}{\partial t} - W \tag{1}$$

where $K_{xx}, K_{yy} \ and \ K_{zz}$ are the hydraulic conductivity values along the x, y and z coordinate axis with the dimensions of length (L) divided by time (T), h is the hydraulic potential head (L), S_s is the specific storage (L^{-1}), W is the volumetric flux per unit volume (T^{-1}).

Conceptual Model

The study area can conceptually be represented by two aquifer units (the Boone and the Ozark) separated by the Chattanooga Shale sandwiched between two confining units (the WICU and the Basement) (Fig. 4). The SRE well injects into the Boone and Hunton formations and the Edgmon well injects into the Arbuckle Group. Therefore, we subdivide the Ozark aquifer into the Hunton and Arbuckle groups.

Model Discretization and Boundary Conditions

We model the area represented in Fig. 1 (by red solid line) and centered at the mid-point of the active Guy–Greenbrier fault for a model domain of 48 km × 40 km in the horizontal plane with the injection wells and faults approximately positioned as indicated on the map. The surface grid discretization varied between approximately 10 m in the proximity of the injection wells and the main faults, to approximately 160 m near the model boundaries. The model top was set to ground surface while the base of the model was defined at 8 km (approximately 2 km below the active section of the Guy–Greenbrier fault). The horizontal hydrogeological layers (Fig. 4) were more highly discretized in the active areas of injection and of seismic activity. Flow across the model's lateral boundaries was simulated via head-dependent flux boundaries. Therefore, the
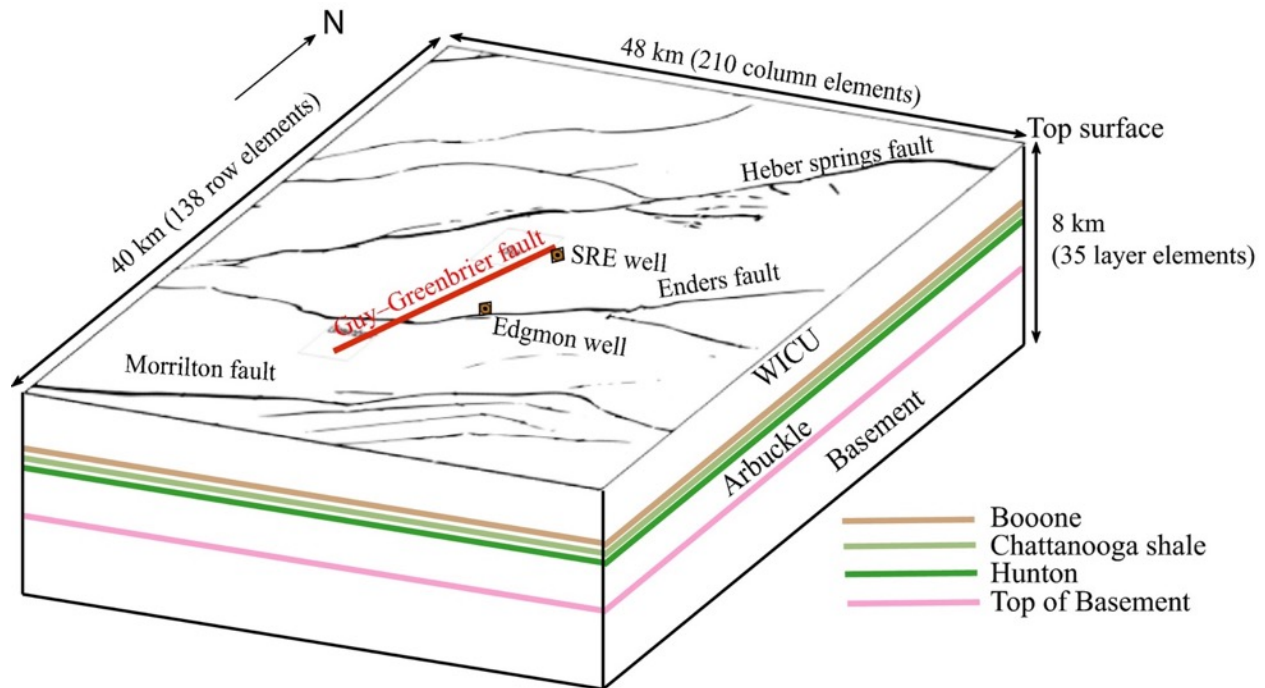
Figure 4: Cartoon of the conceptual model with the dimensions of the modeled area. The main layers consist of Western Interior Confining Unit (WICU), the Boone Formation, the Chattanooga Shale, the Arbuckle Group, and the Precambrian basement.

The conceptual hydrogeological model was translated into a three-dimensional numerical model for simulations using MODFLOW-2005 (Harbaugh 2005). The model comprised the aquifers and confining units up to 8 km depth with layer depths assigned following the stratigraphy of the area by Van Arsdale & Schweig (1990).

groundwater flow was entirely controlled by the injection flux(es) as background (regional) groundwater flow was deemed to be negligible for the duration of the experiment.

Hydrological layers

Following the stratigraphic cross-section (Fig. 2) by Van Arsdale & Schweig (1990), we have incorporated the thinning of layers and the slopes for the sedimentary layers and extended these to the model boundaries. In the vertical direction, the layer thicknesses are based on the stratigraphy and interpretation of well logs. Layers were assumed to be continuous and isotropic throughout the model domain but vary in thickness accordingly.

Faults

We integrated the Morrilton, Enders, and Heber springs faults (Fig. 4) into the model and assigned a uniform hydraulic conductivity over the three faults. The initial properties are those determined below for the Guy–Greenbrier fault and their sensitivity is then tested in the model. For the Guy–Greenbrier fault, we assigned the hydraulic conductivity values estimated below from analysis of the seismicity to the different sections of the fault.

Injection source

Observed daily injection volumes from the SRE well and Edgmon well were the input injection rates. The total simulation time of 348 days covers the complete injection and recovery period at both the SRE and Edgmon wells.

Parameter Estimation: Formation Conductivity

In a pumping test, when the pump is shut down, the water level inside the pumping and observation wells will start to rise. This rise in water level is known as recovery drawdown. Recovery drawdown data can be more reliable for parameter estimation than drawdown data because the recovery occurs at a constant rate, whereas constant discharge pumping is often difficult to achieve in the field. This process can be inverted to have the well inject water into the system then record the falloff of the water/pressure level. The two processes mirror each other. We therefore use a modified water-level recovery scheme (Fig. 5) as the wells are injecting into the aquifers instead of pumping to estimate hydraulic properties of the aquifers.

The SRE well injects in the Boone Formation and Hunton Group, the Trammel well injects in the Boone Formation only, and the Edgmon well injects in the Arbuckle Group. Well-head observations of input pressure and input volume are available at these three wells from the start of injection at each well up to the time of hydrostatic well recovery. The peak tubing pressure and injection volume were sampled every hour in the SRE well and every two hours in the Edgmon well for the entire well record. The peak tubing pressure and injection volume were sampled monthly at the Trammel well between April 2009 and August 2009 and sampled every 2 h after that.

We apply the Agarwal (1980) method to analyze recovery data. The method, based on the Theis well function, defines a recovery drawup s_r and replaces the time axis, during the recovery, by an equivalent time t_e. Agarwal defines the recovery drawup s_r as the difference between the head h at any time during the recovery period and the head h_i at the end of the injection period.

$$s_r = h - h_i \tag{2}$$

The recovery time t_r is the time since the recovery started and is related to the time t since injection started and to the total duration of injection t_i. Considering recovery after a constant rate-injection test, the head h in the aquifer can be expressed with the solution derived by Theis (1935) or can be approximated by the expression derived by Cooper & Jacob (1946). The well dimension and the recovery time permit application of the Theis and Cooper-Jacob method. Using the Cooper-Jacob expression, Agarwal expresses the recovery drawup as:

$$s_r = \frac{Q}{4\pi T} ln \left(\frac{4T}{r^2 S} \frac{t_r t_i}{(t_r + t_i)} \right) = \frac{Q}{4\pi T} ln \left(\frac{4T t_e}{r^2 S} \right) \tag{3}$$

from

$$s_r = \frac{Q}{4\pi T} w(u) \tag{4}$$
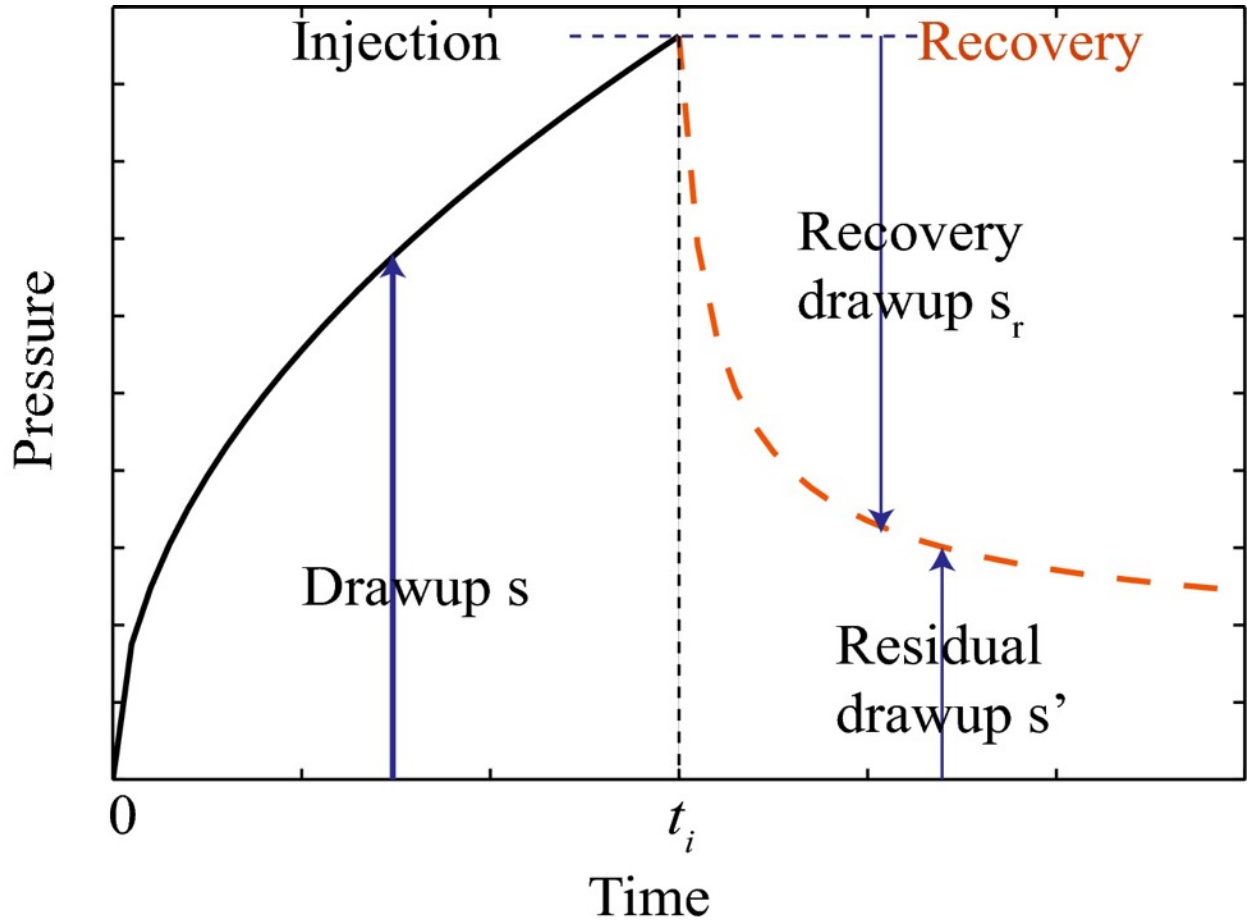
Figure 5: Schematic presentation of a water-level recovery curve.

where Q is rate of injection, T is transmissivity, S is storativity, r is radius of influence, t_e the equivalent Agarwal time expressed as $t_e = \frac{t_r t_i}{(t_r + t_i)}$ and Theis well function $w(u)$ as $u = \left(\frac{r^2 S}{4Tt}\right)$. In this study we use specific weight γ to transform water level s_r to pressure Δp using $\Delta p = \gamma s_r$, and transmissivity to hydraulic conductivity using $T = Kb$ where b is the aquifer thickness.

     Of the three wells, the Theis well function is best suited for the Edgmon well since it injects into a single formation and therefore provides a single fit to the data. We have taken the mean hourly injection rate for the days preceding the shut-in as the injection rate in equation 3, and derived the time periods from the well data. Using the semilog plot (Figure 6A) of t_e vs Δp, we fit the transmissivity and storativity using a forward model scheme by iteratively adjusting the hydraulic parameters to fit the dataset. The transmissivity parameter is mainly sensitive to the gradient of the prediction, while the storativity controls the y-axis intercept. The prediction fits the observed data best for a transmissivity value of 5.7×10^{-5} m^2/hour and storativity value of 1.667×10^{-5}.
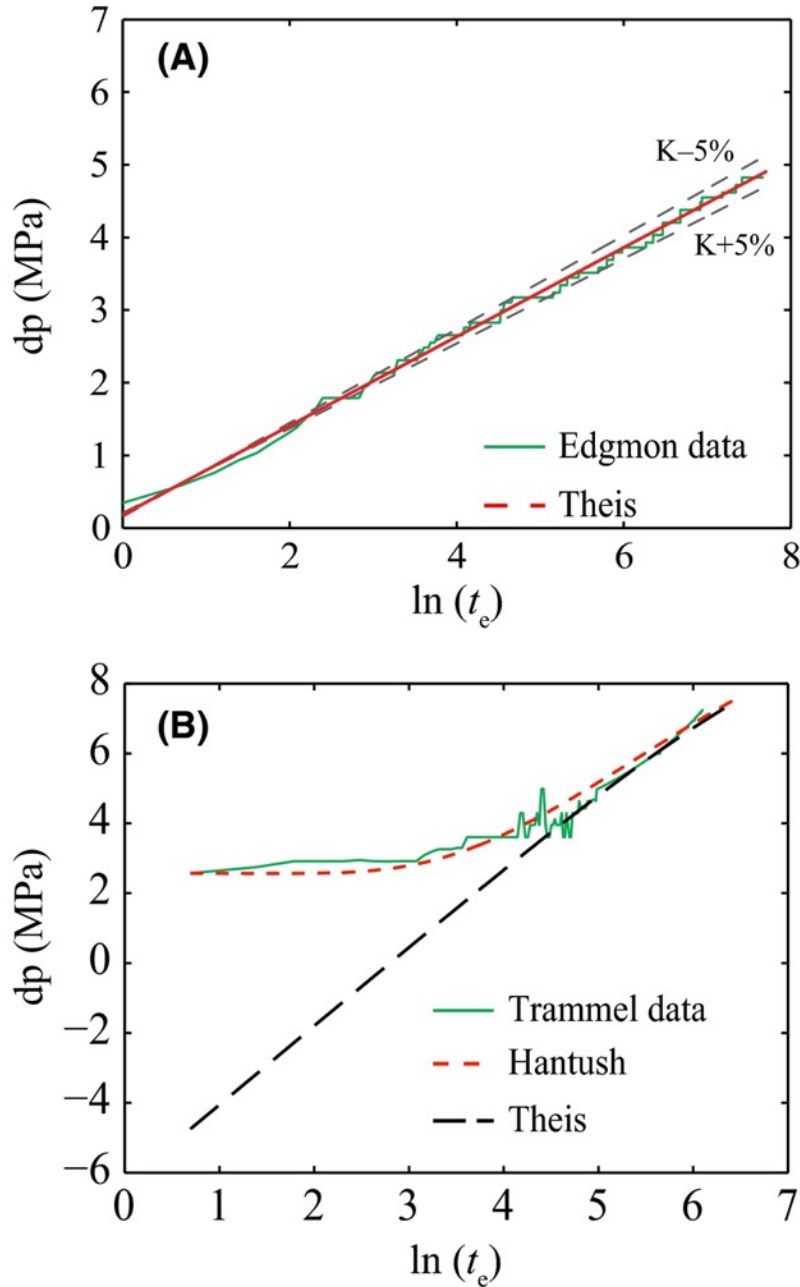
Figure 6: Water-level recovery diffusivity, D, estimate using (A) Theis well function for the Arbuckle Group and the resulting ±5% variation on conductivity, K, and (B) Hantush and Jacob well function for the Boone Formation

For estimation of the hydraulic properties of the Boone, we use the Trammel well since injection occurs only in the Boone. However, the schematics of the well indicate a high percentage of sandstone in the underlying Chattanooga Shale confining unit (Ausbrooks, personal communication) that creates a possible leaky aquifer. Therefore, we apply Hantush-Jacob's method for leaky confined aquifers (Hantush & Jacob 1955) to estimate the properties of the Boone Formation. The Hantush & Jacob (1955) well function for leaky confined aquifers, abbreviated as $w(u, r/B)$ is defined as

$$B = \sqrt{\frac{Tb\prime}{K\prime}} \tag{5}$$

where $b\prime$ is aquitard thickness and $K\prime$ is vertical hydraulic conductivity of the aquitard. Like in the Edgmon well, we use the mean injection rate to perform the forward modeling. The hydrological properties of the Boone Formation fit the high gradient section of the curve while the leaky aquitard controls the flattening of the curve (Figure 6B). The curve fitting provides a transmissivity value of 4.67×10^{-4} m^2/hour and storativity value of 1.67×10^{-4}. The leaky aquitard has a conductivity of 1.52×10^{5}, presenting a highly conductive unit.

Parameter Estimation: Fault Conductivity

Pore-pressure diffusion along a fault or fracture can be characterized by the nature of the permeability. To estimate permeability, Shapiro *et al*. (2002) defined a triggering front based on the time required for the first micro-earthquakes to occur as a function of distance from the well. The pore-pressure diffusion is described by the differential equation

$$\frac{\partial p(t,r)}{\partial t} = D\nabla^2 p(t,r) \tag{6}$$

where D is the hydraulic diffusivity, r the radius vector from the injection point to an observation point, and t is time. In a homogeneous and isotropic medium, the triggering pressure front's radius r is related to time following injection t as

$$r = \sqrt{4\pi Dt} \tag{7}$$

where D is a scalar hydraulic diffusivity. The permeability is calculated from the diffusivity by the formula (Shapiro *et al*. 2003; Economides & Nolte, 2003, chapter 12)

$$k = \frac{\eta\varphi D}{B} \tag{8}$$

where k is hydraulic permeability, η fluid dynamic viscosity, φ is the original porosity of the formation, and B is the bulk modulus of the formation fluid. Since the injection fluid is flowback from hydraulic fracturing, we assume its bulk modulus to be the same as for the formation fluid. We use 2.6 GPa as the bulk modulus based on *Batzle & Wang (1992)*.

We estimate the active fault's diffusivity using the distance–time plot for different sections of the fault. The northern and central section seismicity is associated with injection at the SRE well and begins under the well. However, in order to determine the diffusivity of the fault independent of the timing of the well activity, we take the beginning of first event in the subsequent sections as the start time of the triggering front on the fault, and the hypocenter as the reference origin of pore pressure. The triggering front is interpreted as the curve for Eq. 7 that fits the edge of the seismicity (Fig. 7). We vary the diffusivity in Eq. 7 to find the proper fit. For example, Fig. 7A shows seismicity in the northern section plotted a function of time from the beginning of injection and distance from the SRE well. A diffusivity of 0.23 m^2 sec^{-1} used in
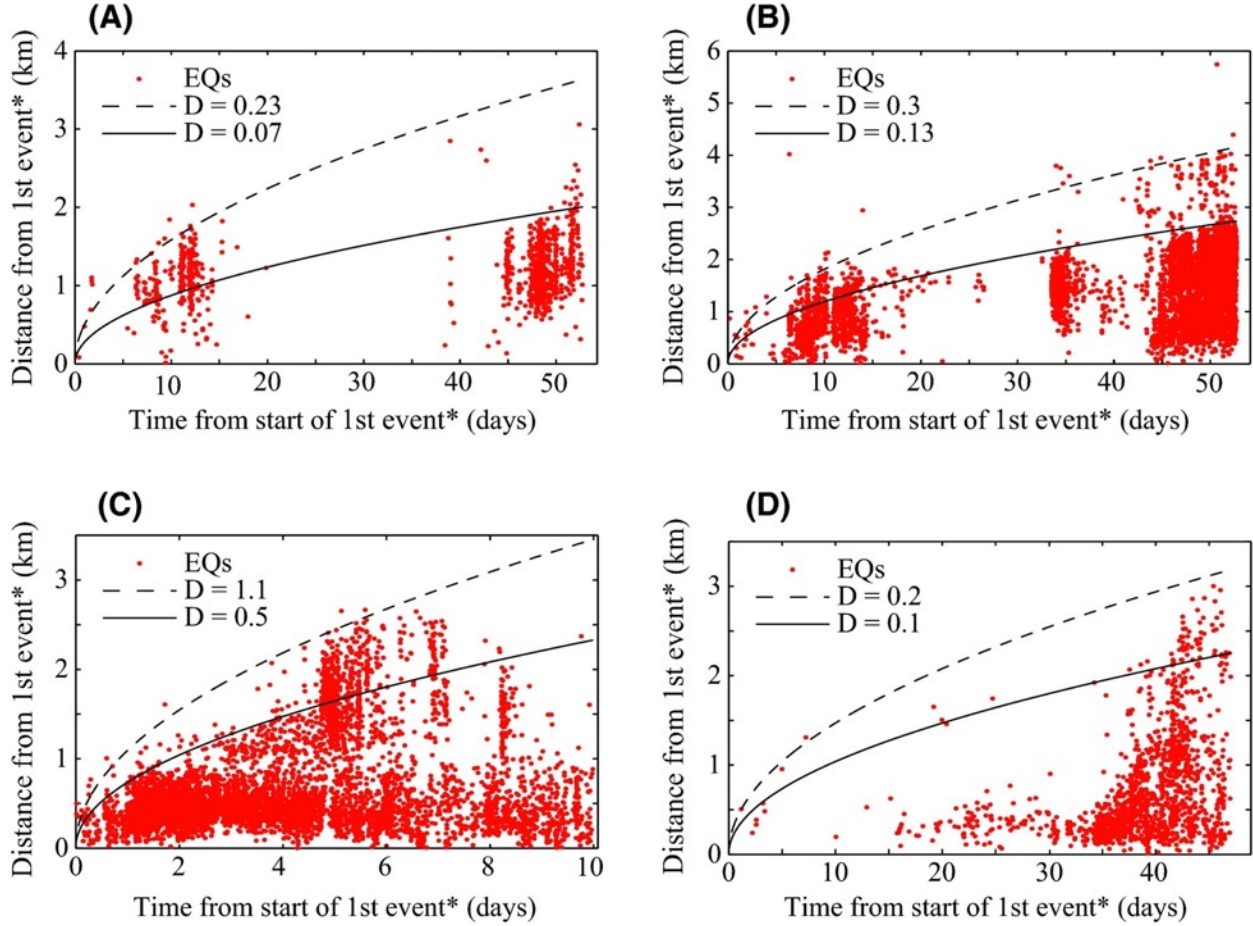
Figure 7: Distances of events (EQs) versus their occurrence time. (A) and (B) are seismicity in the northern and central sections, respectively, while (C) and (D) are seismicity in the southern section above and below 5 km depth, respectively. The reference 1st event is the 1st event in the section attributed to pore-pressure changes from the two wells

Eq. 7 gives the dashed line which bounds the largest distances of the early seismicity in that section. This then is the estimate of diffusivity along the northern section of the Guy–Greenbrier Fault. We then calculate the permeability, and hence the conductivity, of the fault using Eq. 8. Using a porosity of 4% for the Arbuckle Group (Imes & Emmett 1994), we get the conductivity of 0.03 m day^{-1} on the northern section. Using the same procedure for the central section (Fig. 7B) results in the diffusivity of 0.3 m^2 sec^{-1} and the conductivity of 0.04 m day^{-1}.

The southern section has seismicity occurring at a different lithological level, the Precambrian crystalline rock. It starts about halfway between the SRE well and the Edgmon well. We therefore take the start of the seismicity in the section (Fig. 3B) as the start time and the origin point of the triggering pressure front. Seismicity in the southern section is composed of fewer events below 5 km depth that are characterized by higher magnitude (ml > 3) than the shallower events. The seismicity below 5 km depth distinctively begins earlier than the shallower events as seen in Fig. 3B,C, and does not re-occur as much as the shallower events at later time in this section. Following a test of possible diffusivity variation with depth by separately fitting

diffusivity for earthquakes above 5 km depth (Fig. 7C) and below 5 km depth (Fig. 7D), we find the deeper section of the fault has approximately half the conductivity value of the shallower section. Using a porosity of 4%, the shallow section diffusivity (1.1 m^2 sec^{-1}) yields a conductivity value of 0.053 m day^{-1}. The deeper earthquakes are fit better with a diffusivity value of 0.02 m^2 day^{-1} as indicated in Fig. 7D resulting in a conductivity of 0.024 m day^{-1}.

Model Calibration

In the previous section, we used the water-level recovery to estimate the hydrological properties for the Boone Formation and Arbuckle Group. Because the SRE well injects into the Boone Formation and the Hunton Group, we still need to evaluate the hydrological properties of the Chattanooga Shale and Hunton Group. To do this, we run the 3D MODFLOW for the known injection rates while adjusting the hydrogeological properties of the Chattanooga Shale and Hunton Group to best fit the peaks, troughs, and long-term change in pore pressure observed at each well. Figure 8C shows the observed change in hydraulic head (dashed line) at the SRE well with time, and the best fitting prediction. The best fitting conductivity and storativity estimates for the Chattanooga Shale are 1.72×10^{-3} m day^{-1} and 1.0×10^{-5}, respectively, while for the Hunton Group they are 2.2×10^{-2} m day^{-1} and 7.84×10^{-5}, respectively. Figure 8D shows the observation and prediction at the Edgmon well. The pressure fall-off following the shut-in of both wells is also fit well using these values. The horizontal hydrogeological properties of the modeled layers are summarized in Table 1.

We tested the sensitivity of conductivity of the Enders fault in our model. A highly conductive Enders fault propagates pressure into the basement, but more significantly, it allows high pressure diffusion along the Enders fault as shown in Fig. 9A. This creates a pressure buildup on the southern part of Guy–Greenbrier fault close to the Enders fault. Figure 9B shows pressure contours along the Guy–Greenbrier fault assuming a highly conductive Enders fault that indicates pressure buildup from both the northern and southern ends of the Guy–Greenbrier fault. Because seismicity migrated from north to south along the fault, a highly conductive Enders fault is not consistent with the observed seismicity pattern. We reduced the Enders fault's conductivity until the pressure diffusion was not observed along the southern part of Guy–Greenbrier fault at this time. The final model has the 'relatively conductive' Enders fault equal to Arbuckle Group's conductivity.

For a given input, the absolute value of the pore-pressure changes along the Guy–Greenbrier fault is determined by the model parameters. We test the sensitivity by varying the conductivity of each formation by ±25% while keeping the others constant as shown in Table 2. We compare the pressure change at the southern edge of seismicity front at 5 km depth on the Guy–Greenbrier fault on the 106th day of injection with the pressure at that point and time in the initial model. The test results (Table 2) indicate the ±25% change of conductivity in all formations except the Arbuckle Group does not have significant change in modeled pore pressure at the southern edge of seismicity front. A 25% conductivity increase in the Arbuckle Group produces 13% increase in pressure while 25% conductivity decrease produces 16% decrease in modeled pressure. A ± 5% variance in the Arbuckle conductivity (Fig. 6A) produces ±0.6% change in modeled pressure. A test of the relative contribution of each well (last two rows in Table 2) indicates the SRE well contributes approximately 36% and the Edgmon well approximately 64% to the pore-pressure increase at the southern edge of seismicity front in the initial model.
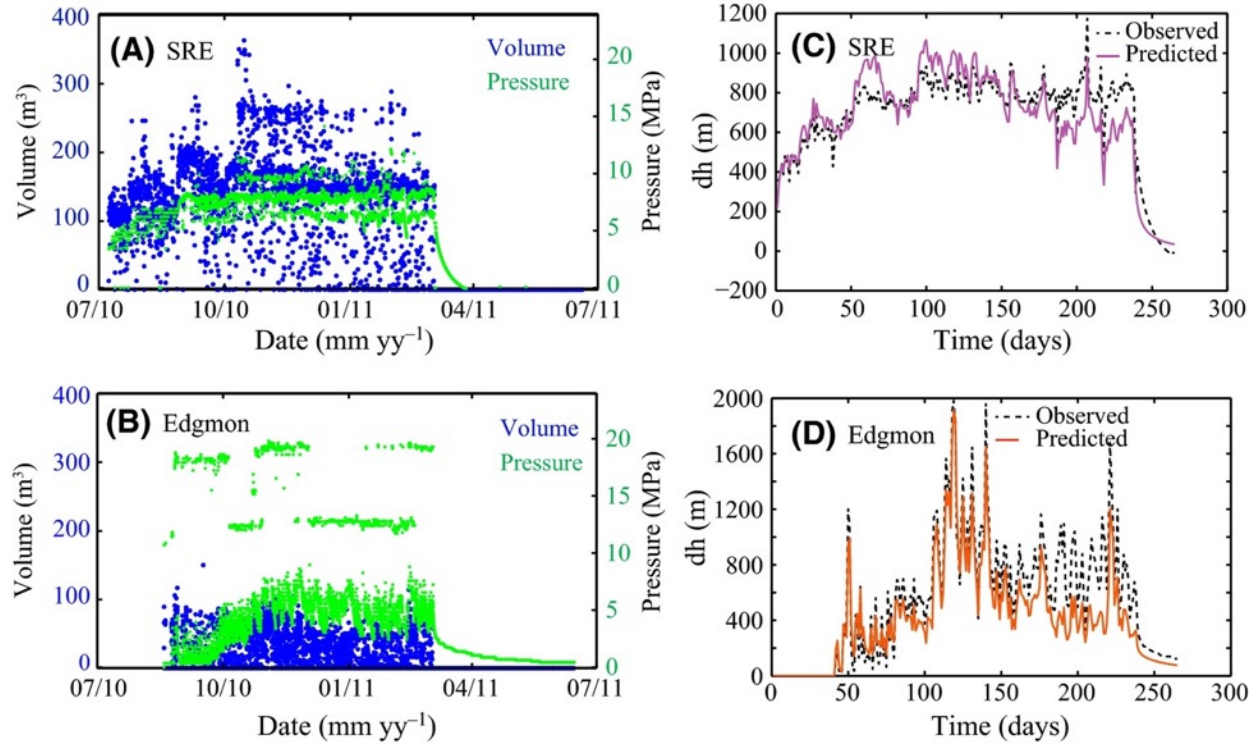
Figure 8: Injection volume and tubing pressure at SRE well (A) and Edgmon well (B) recorded at every two hours and every hour, respectively. Predicted and observed changes in hydraulic head at the SRE well (C) and the Edgmon well (D). The time of injection is with respect to beginning of injection at the SRE well.

Table 1. Hydrogeological properties used in pore-pressure modeling

| Formation/group (source)	Conductivity (m day^{-1}): K	Storativity: S
WICU (Imes & Emmett 1994)	2.0×10^{-4}	1.0×10^{-7}
Boone Formation (water-level recovery)	5.6×10^{-3}	1.67×10^{-4}
Chattanooga Shale (calibration)	1.72×10^{-3}	1.0×10^{-5}
Hunton Group (calibration)	2.2×10^{-2}	7.84×10^{-5}
Arbuckle Group (water-level recovery)	2.03×10^{-3}	1.67×10^{-5}
Basement (Hsieh & Bredehoeft 1981)	2.83×10^{-4}	1.0×10^{-7}
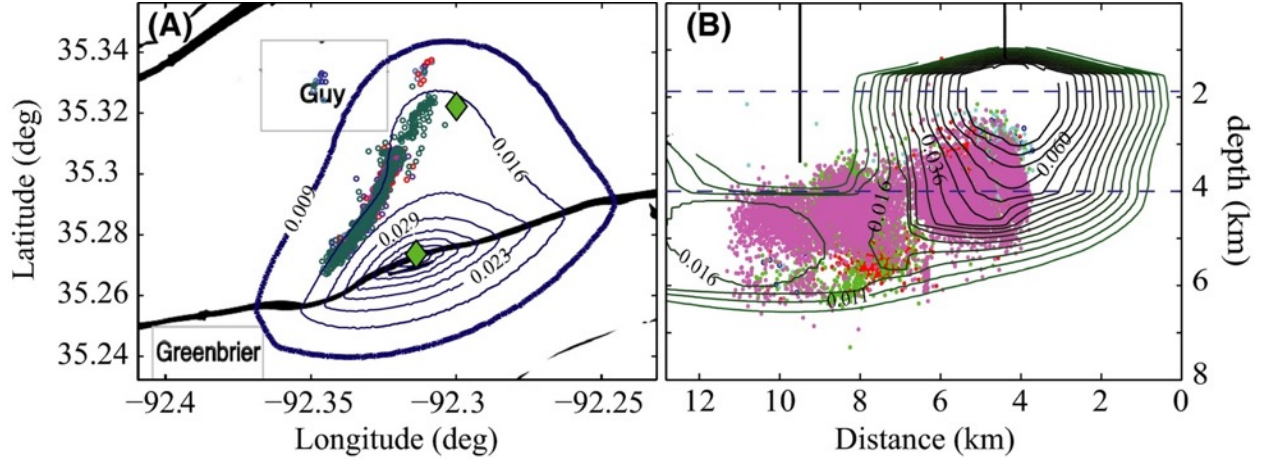
Figure 9: Contours of diffused pore pressure, in MPa, (A) at 5 km depth (in the Precambrian basement) and (B) along the Guy–Greenbrier fault cross-sections with the associated seismicity in the background on the 106th day of injection with respect to SRE well. The model considers a more conductive Enders fault (of equal conductivity to the southern section of the Guy–Greenbrier fault).

We evaluated the sensitivity of the hydraulic conductivity estimate for the Guy–Greenbrier fault by varying the conductivity by one magnitude higher (i.e., X10^1) and one magnitude lower (X10^1) than the derived values. Figure 10 shows comparison of the pressure change at central segment within the Arbuckle (Fig. 10B), around the of start point of seismicity in the southern segment (Fig. 10B), and at the southern endpoint of seismicity within the segment (Fig. 10B) for the modeled period. The results indicate no significant difference (i.e., more than a magnitude) in the pressure change following the variation of conductivity by a factor of ten at the three locations on the fault. We also observe a similarity in pressure increase after varying the fault conductivity.

We lastly implement a depth-dependent hydraulic conductivity across the height of the Ozark aquifer and the basement. A study on Death Valley carbonate deposits by Belcher *et al*. (2001) has shown an apparent linear relation between the logarithmic transform of conductivity and depth. The depth decay of hydraulic conductivity has been expressed by Faunt *et al*. (2004) as:

$$K_{depth}=K_{surface}10^{-\lambda d} \tag{9}$$

where K_{depth} is hydraulic conductivity at depth d, $K_{surface}$ is hydraulic conductivity projected at formation surface, λ is the depth decay coefficient, and d is depth from the formation surface. Applying data from Belcher *et al*. (2001) on the equation, they found a value of $\lambda=1X10^{-5}$ able to reproduce 93% of the original hydraulic conductivity values tested. We use Eq. 9 with the value of $\lambda=1X10^{-5}$ to extrapolate depth-dependent hydraulic conductivity in the Ozark aquifer and the basement.
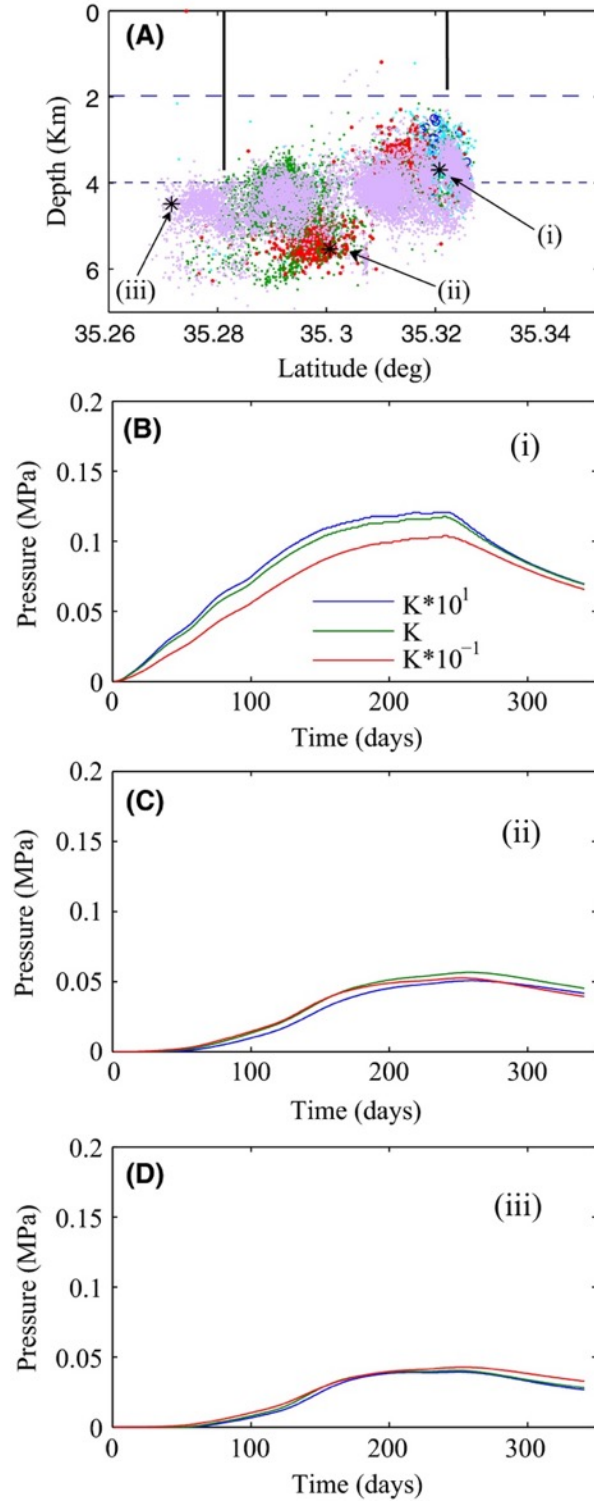
Figure 10: Comparison of pressure change over time (B, C, and D) at different locations along the Guy–Greenbrier fault (asterisks in A) showing the sensitivity of hydraulic conductivity values assigned to the fault.

Table 2. Varying conductivities (bold) and the associated effect on pore-pressure increase at the southern edge of seismicity on the Guy–Greenbrier fault on the 106th day of injection with respect to SRE well

| Boone $\times 10^{-3}$ (m/day)	Chattanooga $\times 10^{-3}$ (m/day)	Hunton $\times 10^{-2}$ (m/day)	Arbuckle $\times 10^{-3}$ (m/day)	Basement $\times 10^{-4}$ (m/day)	SRE well (on)	Edgmon well (on)	Pressure (MPa)
5.60	1.72	2.20	2.03	2.83	yes	yes	0.00806
7.00	1.72	2.20	2.03	2.83	yes	yes	0.00825
4.20	1.72	2.20	2.03	2.83	yes	yes	0.00833
5.60	**2.15**	2.20	2.03	2.83	yes	yes	0.00823
5.60	**1.29**	2.20	2.03	2.83	yes	yes	0.00837
5.60	1.72	**2.75**	2.03	2.83	yes	yes	0.00824
5.60	1.72	**1.65**	2.03	2.83	yes	yes	0.00832
5.60	1.72	2.20	**2.55**	2.83	yes	yes	**0.00937**
5.60	1.72	2.20	**1.53**	2.83	yes	yes	**0.00701**
5.60	1.72	2.20	2.03	**3.54**	yes	yes	0.00829
5.60	1.72	2.20	2.03	**2.12**	yes	yes	0.00828
5.60	1.72	2.20	2.03	2.83	yes	**NO**	**0.00292**
5.60	1.72	2.20	2.03	2.83	**NO**	yes	**0.00521**

Results

We present results for the pore-pressure model and compare these to the spatial and temporal occurrence of seismicity on the Guy–Greenbrier fault. We show pressure change around seismically active area of the Guy–Greenbrier fault (yellow dashed line in Fig. 1) during the analyzed period. Injection starts first at the SRE well and 41 days later at the Edgmon well (Fig. 8). Therefore, we have referenced our time period to the beginning of injection at the SRE well. The pressure change generally propagates radially away from the injection wells during the initial pressure diffusion period except where a fault is encountered as shown in Fig. 11A. The pressure gradient decays away from the injection wells during the injection period with the highest pressure increase experienced closest to the wells (Fig. 11A,B). Figure 8A,C shows that during the period of injection, the pressure increases gradually within the formation and levels off after approximately 56 days of injection around the SRE well. At the Edgmon well shown in Fig. 8B,D, pressure starts building up on the 75th day (i.e., day 34 of injection at the Edgmon well) and flattens on the 125th day (i.e., day 84 of injection at the Edgmon well). Away from the injection wells, the pulse response at the wells is smoothed with distance through the aquifer such that the aquifer acts as a low pass filter to the pressure signal.

The pressure fronts following a period of injection interact with each other additively to increase the pressure at the points of interaction. During the diffusion period, the pressure contours are distorted at the fault contact where the diffusivity values change. The pressure diffusion contours follow the direction of the fault such that below the injection level of the SRE well, the highest pressure is experienced along the Guy–Greenbrier fault and decays away from the fault (Fig. 11A). In both wells, the faults feed pressure to the underlying formation faster than the aquifer itself.

Pressure at 5 km depth surface

The map view of pressure diffusion provides an understanding of the interaction of pressure from the two wells (Fig. 12). We present the pore-pressure change at 5 km depth because much of the seismicity occurs at that depth across the whole Guy–Greenbrier fault. Seismicity begins at this depth following 82 days of injection in the SRE well (i.e., 41 days of injection in the Edgmon well), and the model results indicate the propagating pressure front is dominantly from the SRE well (Fig. 12A). Later, despite the interaction of the two wells (Fig. 12A–C), pressure change at 5 km and below is dominated by the injection at the Edgmon well. At 5 km depth, pressure changes due to injection at the SRE well are low but spread over a larger surface compared with the Edgmon well. The northern and central sections of the fault help transport pressure to the basement, and in this area, the pressure is centered along those fault sections. Further south, the proximity of injection at the Edgmon well to the basement and the penetration of the Enders fault into the basement creates a higher pressure gradient at 5 km depth within a short lateral distance of the well. The relatively conductive Enders fault acts as a secondary source of pore pressure to the southern part of the Guy–Greenbrier fault. At the 5 km depth, following the initiation of seismicity in the basement (Fig. 12A), seismicity appears to migrate both north and south along the Guy–Greenbrier fault from that starting point. The model indicates higher pressure changes accompanying the northern migration as compared to the southern migration (Fig. 12B–D). As seen below, seismicity on the fault actually starts at 3.5 km depth directly under the SRE well on day 58. Seismicity actually migrates from north to south along the Guy–Greenbrier fault.
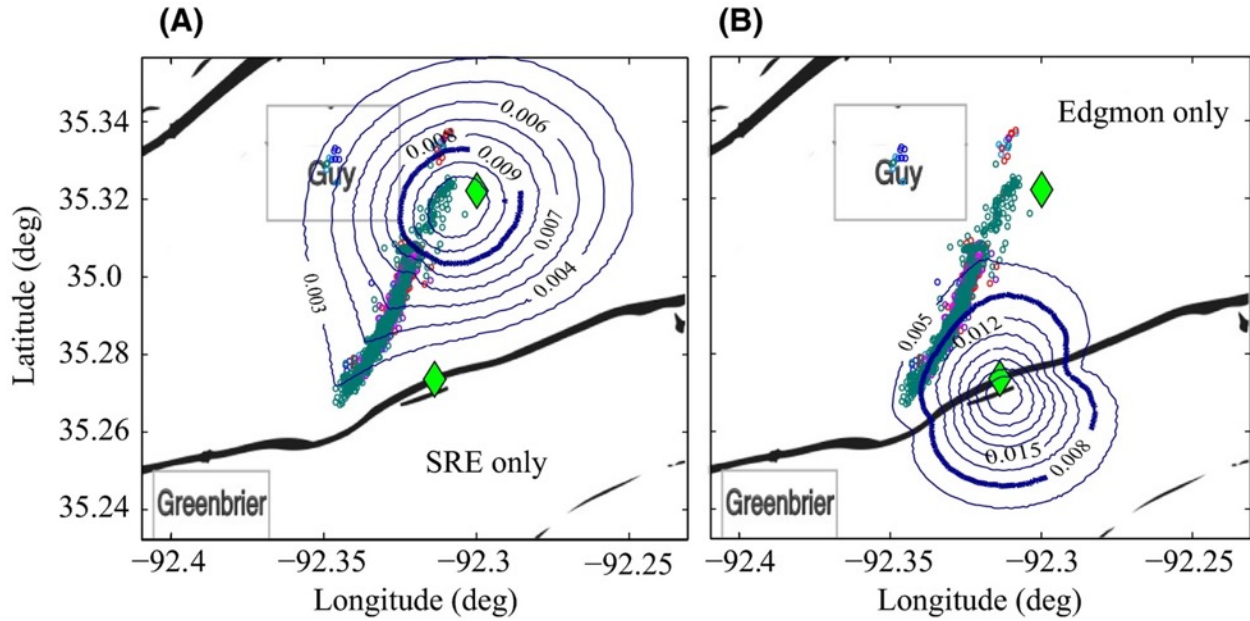
Figure 11: Contours of pore-pressure changes, in MPa, at 5 km depth (in the Precambrian basement) and the corresponding seismicity located at >=5 km depth in the background after 106 days of injection with respect to SRE well. This is a case scenario of injection at (A) SRE well only and (B) Edgmon well only.

Pressure along the Guy–Greenbrier fault

In Fig. 13, we present the vertical cross-sectional modeling results along the Guy–Greenbrier fault for five significant periods of injection as defined by the spatiotemporal evolution of seismicity. Note that the SRE well is close to the plane of the fault but the Edgmon well is approximately 2.5 km off the fault. This distorts the appearance of the contours on the fault.

After 58 days of injection, Fig. 13A shows larger lateral pore-pressure changes in the Ozark aquifer than the shallower Boone Formation aquifer. Pressure changes within the Boone Formation are minimal due to the high conductivity of the formation that does not allow pressure buildup. The radial flow contours from the SRE well observed north of the well are slightly elongated along the fault to the south at this time.

The earthquakes in Fig. 13A are on the fault. The pressure contours at the distance limit of seismicity around the SRE well suggest a minimum pore-pressure increase of approximately 0.037 MPa is sufficient to induce seismicity within the sedimentary units along the Guy–Greenbrier fault (Fig. 13A). At this time of injection, it is clear that most of the pressure change from the SRE well is in Ozark aquifer along the northern and central sections of the fault. Even though injection at the Edgmon well has begun, it is apparent that the seismicity at this time is related to the SRE well.

By day 82 as pressure continues to increase in the Ozark aquifer along the north and central sections of the fault, we see the beginning of interaction between the 0.007 MPa pore-pressure fronts from the two wells (Fig. 12A). Figure 13B also shows pressure changes that are confined largely to the Precambrian basement extending along the southern section of Guy–
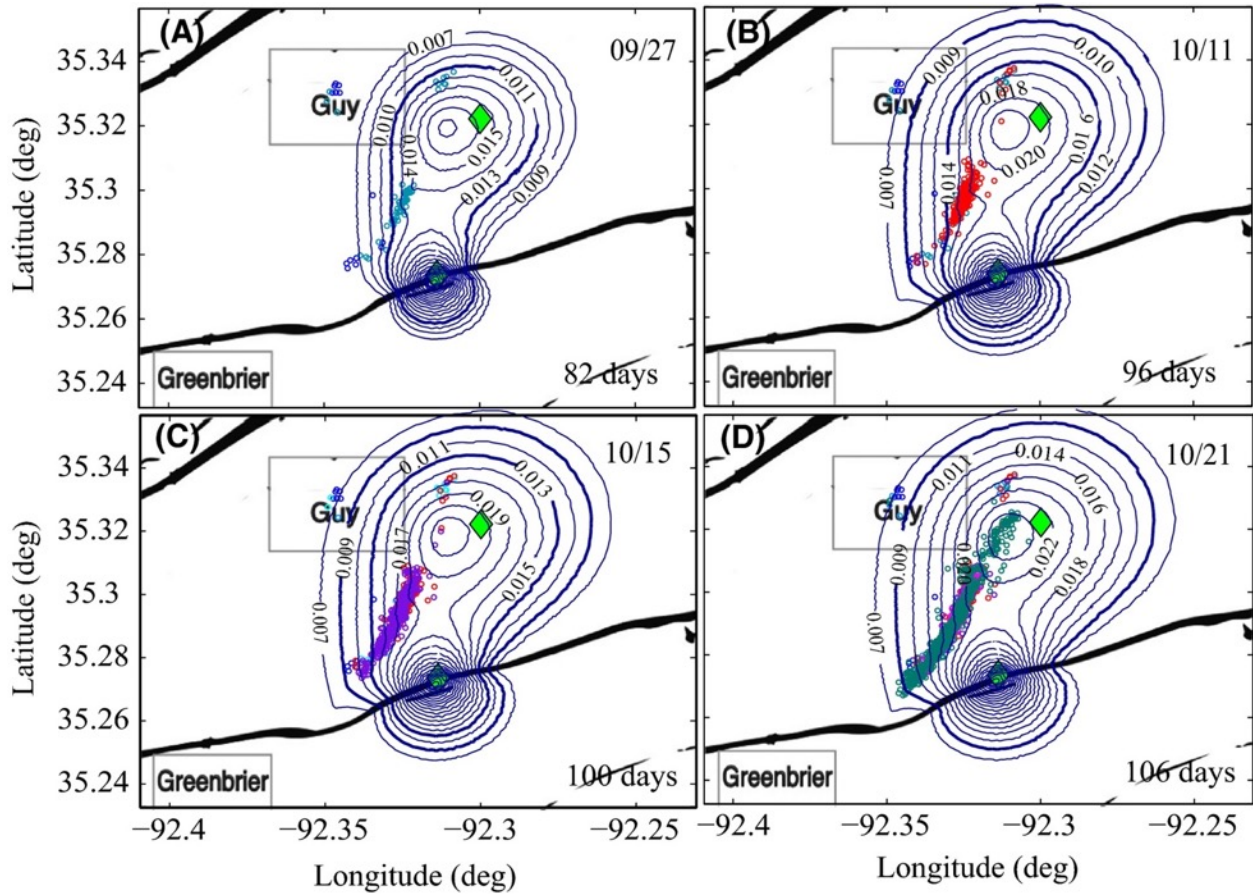
Figure 12: Contours of pore-pressure changes, in MPa, at 5 km depth (in the Precambrian basement) and the corresponding seismicity located at >=5 km depth for (A) 82 days, (B) 96 days, (C) 100 days, and (D) 106 days of injection with respect to the SRE well. The diamonds are injection wells.

Greenbrier fault. These pressure changes in the basement result from radial flow from the Edgmon well adding to channeled flow along the fault from the SRE well. The pressure contours indicate that the start of seismicity within the basement fault section at this time requires a minimum of approximately 0.009 MPa pore-pressure change. At the same time, the rate of seismicity increases within the northern and central sections. The leading edge of the seismicity on the central section fits the approximately 0.055 MPa contour (Fig. 13B). Seismicity following the approximately 0.055 MPa pore-pressure contour seems consistent within the central section as injection continues (Fig. 13C,D).

As in the central section, the leading edge of seismicity on the southern section follows two fronts of pressure contours. Initial low-level seismic activity tends to follow the approximately 0.009 MPa pressure front (Fig. 13B–D) while a more intense episode of seismicity follows the approximately 0.012 MPa pressure contour. Unlike in the central section where the leading seismicity occurred almost evenly across the depth of the fault section, the leading seismicity in the southern section occurs at the deeper section of the fault with shallower seismicity lagging behind (Fig. 13D,E). Through this time period, it is apparent that the minimum triggering pressure in the sedimentary formation is higher than in the basement. The
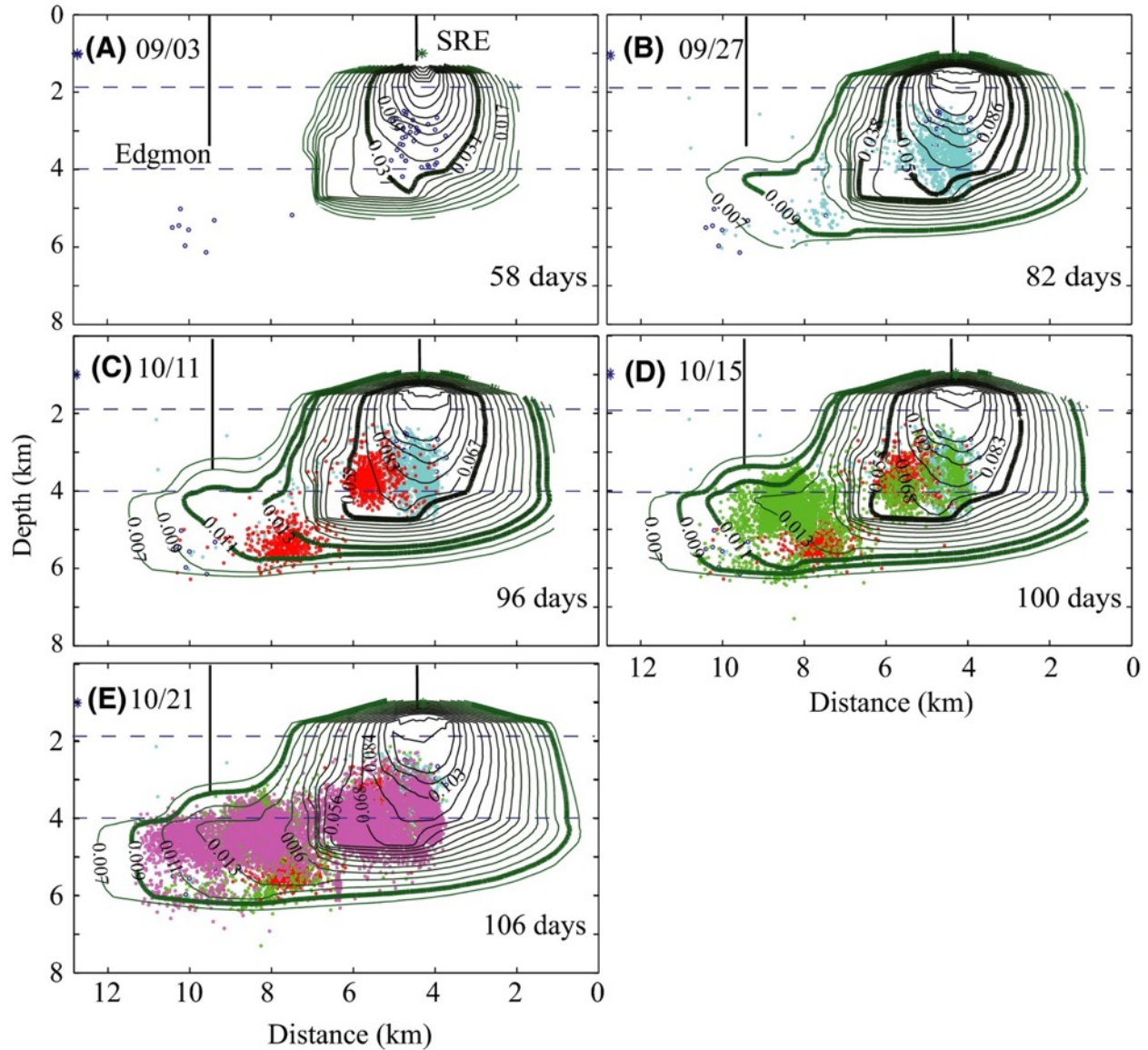
Figure 13: Contours of diffused pore pressure, in MPa, along the Guy–Greenbrier fault cross-sections with the associated seismicity in the background. The cross-sections correspond (A) 58 days, (B) 82 days, (C) 96 days, (D) 100 days, and (E) 106 days of injection with respect to the SRE well. The dots are earthquakes located on the fault. The dashed horizontal lines indicate the confines of the Ozark aquifer.

vertical extent of pore-pressure changes into the crystalline basement is restricted by the reducing conductivity of the basement.

Discussion and Conclusion

The magnitude of pore-pressure change enough to induce seismicity at a given point is partly dependent on the proximity of the injection well and the connectivity between the point of injection and the point of failure. Injection in the study area occurs at different depths. At the

SRE well, injection targets a fractured anticline zone where hydraulic conductance is relatively high. Fluids are injected into the Boone Formation and Hunton Group spanning an injection depth of approximately 70 m with perforations evenly distributed. On the other hand, although the perforated well screen in the Edgmon well covers an interval of approximately 900 m, about 80% of the perforations are located in the bottom 300 m of the well. This essentially means most of the injection is concentrated near the top of the basement and therefore pressure buildup is higher at depth than it would be if injection was evenly spread across the approximately 900 m of well screen.

Modeled parameters

Calibration of the Ozark confining unit and the Hunton Group yields conductivity values of 1.72×10^{-3} m day^{-1} and 2.2×10^{-2} m day^{-1}, respectively. The calibration conductivity of the Chattanooga Shale (i.e., 1.72×10^{-3} m day^{-1}) is close to the 5.0×10^{-4} m day^{-1} value estimated by Imes & Emmett (1994) as the vertical conductivity. On the other hand, the conductivity is much higher than the 2.02×10^{-7} m day^{-1} determined from core analysis of Chattanooga Shale in Alabama (Pashin *et al.* 2011). This higher conductivity we determined can partly be attributed to a fracture network within the formations and to the high percentage of sandstone. The semiconductive Ozark confining unit consequently links the Boone Formation and the Hunton Group and limits lateral pressure buildup within the Boone Formation whose thin (36 m) geometry would seem to provide a favorable condition for pressure buildup. Stanton (1993) estimates the conductivity of the Boone Formation to be 0.76 m day^{-1}, but this could vary depending on secondary porosity developed through dissolution along faults, fractures, and bedded plains (Imes & Emmett 1994). Imes & Emmett (1994) model the Boone using a conductivity value of 6.6 m day^{-1}. We prefer the lower range of conductivity estimated from the water-level recovery over the higher values from Stanton (1993) and Imes & Emmett (1994) because the higher values produce a draining system that does not allow the observed pressure buildup around the SRE well.

Pore-pressure change around the wells

Pressure history during the two well operation period has provided important input to the model parameter estimation and the model calibration. Injection is not continuous at either well and so hourly tubing pressure records show the input pressure during injection and also the buildup of aquifer pressure between injection periods (Fig. 8A,B). The pressure plot importantly shows the pressure change in the formation as elaborated by the noninjection period of the well. The plot indicates that injection at shallower depth of the Ozark aquifer (i.e., SRE well) is sustainable at lower pressure for higher volume compared to injection at deeper section of the aquifer (i.e., Edgmon well).

Pressure increase as well as decay occurs at different rates at the two wells. The SRE well shows a consistent increase in the pore-pressure change from the onset of injection (Fig. 8A). On the other hand, there is a approximately 34-day period in the Edgmon well where the pore-pressure change level remains level before a consistent gradual increase (Fig. 8B). Later on in both wells, the observed pressure change reaches a plateau after a approximately 55-day buildup in the SRE well and a approximately 44-day buildup in the Edgmon well. The difference in the timing of pressure change buildup can partly be attributed to the sustained higher injection rate or volume at the SRE well compared to the Edgmon well. In the calibration, modeling using the inferred model properties fits the well history up to 150 days before the pressure levels dip in the

model (Fig. 8C,D). Model results (Fig. 12B–D) show evident interaction of pressure increase from the two wells following 82 days of injection in the SRE well (i.e., 41 days of injection in the Edgmon well). It is important to note that several wells started injecting earlier than the two wells studied (Horton 2012) and a similar elevated pressure interaction is possible from the other wells. In a case where several wells contribute to the aquifer pressure elevation and the pressure level has reached the plateau, it is possible to sustain higher pressure levels with a slightly reduced injection rate for a short time.

Role of Enders fault
        The geometry of Enders fault and similar faults that cut through the aquifers into the basement plays a significant role in introducing pressure changes to the basement. For example, a test shows that less pressure increase is experienced in the basement when injection occurs at the Edgmon well for a nonpenetrative Enders fault (the fault does not connect the Ozark and the Precambrian). One reason for less pressure increase is that permeability has been set to one order of magnitude lower in the vertical direction compared to lateral directions (Stanton 1993) in addition to its decay with depth in the basement. This translates to low conductance that limits the effective depth of pore-pressure changes. A more permeable and conductive fault that penetrates into the basement becomes a medium for pressure propagation into the basement (Fig. 9A). The elevated pressure then diffuses laterally depending on the lateral conductivity of the basement and the Arbuckle Group. In the study area, by injecting fluids near the Enders fault at elevated pressure introduces pressure changes into the basement that eventually diffuse laterally into the Guy–Greenbrier Fault as seen from the model (Fig. 12B–D). The best fitting model for the Enders fault has hydrological characteristics equal to the sedimentary units. A more permeable Enders fault within the sedimentary units propagates pressure faster along the fault and thereby increases pressure in the Guy–Greenbrier fault at the point where the two faults intersect just NE of Greenbrier city (Fig. 9A). Such a model does not fit the seismicity as pressure would migrate northward along the southern part of the fault while seismicity migrates southwards (Fig. 9A,B). We postulate that cementation has occurred in the Enders fault and that the conductivity gradient between the cemented fault and the crystalline basement is sufficient to allow pressure propagation into the basement. Caplan (1960), on the basis of samples from six wells in northwest Arkansas, describes the St Francois aquifer (missing in the study area) to be loosely cemented with the underlying Precambrian rocks at its base. Such cementation could have occurred to the faults cutting into the basement.

Seismogenic permeability
        Hydraulic permeability plays a major role in pore-pressure diffusion. Talwani *et al*. (2007) introduced a seismogenic permeability ks that can permit pore-pressure diffusion in fractures. Most of his ks values were derived from estimated diffusivity parameters in other studies. While permeability lower than ks provides an undrained response, higher permeability produces a drained response. The absence of coupling in both cases limits pore-pressure diffusion. In this study, the Boone's permeability is high such that it drains off the injected fluids, while at the same time, the basement's permeability reduces with depth, thereby limiting drainage rate. The Boone and the deeper stratigraphy of the basement experience the least pore-pressure changes in the model. It is within the Ozark aquifer, the Guy–Greenbrier fault, and the top stratigraphic layer of the basement where pore-pressure elevation is experienced. The diffusivity of the hydrogeological units where pore-pressure effectively diffuses ranges between

0.1 and 1.1 m^2 sec^{-1} and fits within the range of 0.1–10 m^2 sec^{-1}, which seems appropriate for many cases of induced seismicity as analyzed by Talwani *et al*. (2007).

Triggering pressure front

We found the minimum pore-pressure increase needed to induce seismicity on the Guy–Greenbrier fault is 0.009–0.012 MPa within the crystalline Precambrian basement and 0.035–0.055 MPa in the Arbuckle Group. Keranen *et al*. (2014) have suggested a minimum of approximately 0.07 MPa pore-pressure changes in the Arbuckle Group in Oklahoma. Although there is a small difference, it is important to note the relation between the triggering pressure and earthquake magnitude. In this study, we use an earthquake catalog that is complete up to ml=0. With the smaller earthquakes (i.e., ml < 2) preceding the larger ones, the threshold pressure of the triggering front becomes dependent upon the magnitude of the earthquakes used for interpretation. Rothert & Shapiro (2007) analyzed injection-induced microseismicity in the magnitude range −2 < Mw < 2.7 from the Hot Dry Rock experiment tests in crystalline rocks and a hydraulic fracturing experiment in a sedimentary rock. They found pressure changes in the low range of 0.001–1 MPa sufficient to induce seismicity.

Effective stress variation

According to the Mohr–Coulomb criterion for slip, an increase in pore pressure reduces the effective stress and thereby brings a fault closer to shear failure. Reduced effective stress leads to critically stressed regimes, which is a prerequisite for earthquakes triggered by the pore-pressure mechanism (Healy *et al*. 1968). The amount of pore-pressure increase required to induce seismicity is therefore dependent on the preexisting effective stress and the orientation of the fault. Zoback & Townend (2001) have postulated that the upper and lower crust and lithospheric mantle are totally coupled and that the total strength of intraplate lithosphere must equal the imposed plate tectonic stress while the pore-pressure gradient is hydrostatic. They suggest that intraplate regions are in a state of failure equilibrium based on induced and triggered seismicity and *in situ* stress measurements. This equilibrium is controlled by the frictional strength of the preexisting faults, and can be expressed as the ratio of the maximum and minimum principal effective stresses that is limited to 3.1 above which failure occurs (Zoback 2007). As the principal effective stresses increase with depth in a strike-slip regime, the maximum principal effective stress gradient is greater than that of the minimum principal effective stress. The increase in the difference between the principal effective stresses with depth brings the frictional equilibrium closer to failure. As the frictional equilibrium gets closer to failure with increasing depth, an increase in pore-pressure will perturb the equilibrium system by reducing the magnitude of the effective stresses and thereby inducing failure. The magnitude of the pore-pressure change enough to induce failure is therefore dependent on the depth of the fault as supported by the reduced initiation pore pressure with depth experienced in this study. Zoback & Zoback (1991) suggests the principal compression axis of the present-day stress field in the mid-continent is in the ENE orientation. In this state and orientation of stress in mid-continent, the approximately N30E orientation of the Guy–Greenbrier fault favors a strike-slip failure when pore pressure is elevated.

In summary, we have developed a pore-pressure model to explain the beginning and migration of the Guy–Greenbrier fault seismicity. The continued injection of the two wells shows an interaction and buildup of pore pressure along the Guy–Greenbrier fault with the pressure front and seismicity migrating from north to south along the fault. The conductivity of

the Precambrian basement faults plays a key role in diffusion of pore pressure especially with the Enders fault channeling pore pressure to the basement from the overlying Ozark aquifer. The magnitude of the pore-pressure triggering front is dependent on many factors and the critical triggering threshold interpretation can be dependent upon to earthquake location especially where the micro-earthquakes precede moderately sized earthquakes. We found the minimum pore-pressure increase needed to induce seismicity on the Guy–Greenbrier fault is 0.009–0.012 MPa within the crystalline Precambrian basement and 0.035–0.055 MPa in the Arbuckle Group, and a ±5% variance in the Arbuckle conductivity produces ±0.6% change in modeled pressure in the basement along the Guy–Greenbrier fault.

References Cited

Agarwal RG (1980) A new method to account for producing time effects when drawdown type curves are used to analyze pressure buildup and other test data, Presented at the Society of Petroleum Engineers Annual Technical Conference and Exhibition, Sept.21-24, Dallas, SPE paper 9289.

Barton CA, Zoback MD, Moos D (1995) Fluid flow along potentially active faults in crystalline rock. *Geology*, **23**, 683–686.

Batzle M, Wang Z (1992) Seismic properties of pore fluids. *Geophysics*, **57**, 1396-1408.

Belcher WR, Elliott PE, Geldon AL (2001) Hydraulic property estimates for use with a transient ground-water flow model of the Death Valley regional ground-water flow system, Nevada and California: U.S. Geological Survey Water Resources Investigations Report 01–4210, 28 p.

Burke, K., and Dewey, J. F. (1973). Plume-generated triple junctions: Key indicators in applying plate tectonics to old rocks. *Geology* 81, 406–433.

Caplan, W. M. (1954). Subsurface Geology and Related Oil and Gas Possibilities of Northeastern Arkansas. Arkansas Resources and Development Commission Bulletin no. 20, 124 pp

Caplan WM (1960) Subsurface Geology of pre-Everton Rocks in Northern Arkansas. Arkansas Resources and Development Commission information circular no. 21, 17 pp.

Chiu, J. M., Johnston, A. C., Metzger, A. G., Haar, L., and Fletcher, J. (1984). Analysis of Analog and Digital Records of the 1982 Arkansas Earthquake Swarm, *Bull. Seismol. Soc. Am.* 74, 1721-1742.

Cooper HH, Jacob CE (1946) A generalized graphical method for evaluating formation constants and summarizing well field history. *American Geophysical Union Transactions,* **27**, 526-534.

Economides MJ, Nolte KG (2003) Reservoir Stimulation, pp. 5.1 – 5.14, John Wiley, Hoboken, N. J.

Ellsworth WL, Hickman SH, Lleons AL, Mcgarr A, Michael AJ, Rubinstein JL (2012) Are seismicity rate changes in the midcontinent natural or manmade? (Abstract). *Seismological Society of America Annual Meeting*, **83** (12), 137.

Frohlich C (2012) Two-year survey comparing earthquake activity and injection-well locations in the Barnett Shale, Texas. *Proceedings of the National Academy of Sciences*, **109**(35), 13934–13938.

Gutenberg, R., and Richter, C. F. (1944). Frequency of earthquakes in California. *Bull. Seismol. Soc. Am.* 34, 185-188.

Hantush MS, Jacob CE (1955) Non-steady Radial Flow in an Infinite Leaky Aquifer. *Transactions, American Geophysical Union*, **36**(1), 95–100.

Harbaugh AW (2005) MODFLOW-2005, The U.S. Geological Survey modular ground-water model -- the Ground-Water Flow Process: U.S. Geological Survey Techniques and Methods 6-A16, variously p.

Healy JH, Rubey WW, Griggs DT, Raleigh CB (1968) The Denver earthquakes. *Science*, **161** (3848), 1301 – 1310.

Horton S (2012) Disposal of hydrofracking waste water fluid by injection into subsurface aquifers triggers earthquake swarm in Central Arkansas with potential for damaging earthquake. *Seismological Research Letters*, **83** (2), 250 – 260.

Horton, S. P., Ogwari, P., and Ausbrooks, S. (2013). Naturally Occurring and Induced Earthquakes in Central Arkansas (Abstract), *Seismol. Res. Lett.* 85, 214-241.

Horton, S. , S. Ausbrooks, M. Withers and P. Ogwari, Managing Seismic Hazard Due to Induced Earthquakes in Central Arkansas through Partnership between Scientific and Regulatory Agencies, at SSA Annual Meeting 2014

Hsieh PA, Bredehoeft JD (1981) A reservoir analysis of the Denver earthquakes: A case of induced seismicity. *Journal of Geophysical Research*, **86** (2), 903–920.

Imes JL, Emmett LF (1994) Geohydrology of the Ozark Plateaus Aquifer System in Parts of Missouri, Arkansas, Oklahoma, and Kansas. USGS Professional Paper 1414-D.

Ishimoto, M., and Iida, K. (1939). Observations of earthquakes registered with the microseismograph constructed recently, *Bull. Earthq. Res. Inst*. 17, 443–478.

Kissling E. (1995). Velest User's Guide. Int. Report, Inst. Geophysics, ETH Zurich, 1-26

Keranen K, Savage HM, Abers GA, Cochran ES (2013) Potentially induced earthquakes in Oklahoma, USA: Links between wastewater injection and the 2011 Mw 5.7 earthquake sequence. *Geology*, **41** (6): 699-702.

Keranen KM, Weingarten M, Abers GA, Bekins BA, Ge S (2014) Sharp increase in central Oklahoma seismicity since 2008 induced by massive wastewater injection. *Science*, **345** (6195), 448-451.

Lancaster, G. (2011). "Red River." Encyclopedia of Arkansas History and Culture.. http://www.encyclopediaofarkansas.net/encyclopedia/media-detail.aspx?mediaID=6333 (accessed October 16, 2015)

Lee, W. H. K., and Stewart, S. W. (1981). Principles and Applications of Microearthquake Networks, *Advances in Geophysics*, Supplement No. 2, Academic Press, New York, 293 pp

Nicholson C, Wesson RL (1990) Earthquake hazard associated with deep well injection: a report to the U.S. Environmental Protection Agency. *United States Geological Survey Bulletin*, **1951**, Reston, Virginia: USGS.

Ogwari, P. O., and S. P. Horton (2013), Using induced earthquakes to estimate hydraulic properties of subsurface reservoirs in central Arkansas, Annual Meeting of the Seismological Society of America, Salt Lake City, UT, *Seismological Research Letters* **84**, p. 375.

Ogwari, P.O., and S. Horton (2015), A 3D Model of Pore Pressure Diffusion Associated With Induced Seismicity in Guy, Arkansas, *Seismological Research Letters* **86** (2015).

Ogwari PO, Horton S, Ausbrooks S (2016) Characteristics of Induced/Triggered Earthquakes During The Early Phase of The Guy-Greenbrier Earthquake Sequence in North-Central Arkansas. *Seismological Research Letters*, **87**, 620-630.

Ogwari P., and Horton S. (2016), Spatiotemporal analysis of the 2010-2011 Guy-Greenbrier sequence and the associated pore-pressure beyond fluid disposal period, SSA (2016).

Ogwari, P.O., and S. Horton, Numerical Model of Pore Pressure Diffusion Associated with the Initiation of the 2010-2011 Guy-Greenbrier, Arkansas Earthquakes, *Geofluids* **16**, 954-970.

Pashin JC, Kopaska-Merkel DC, Arnold AC, McIntyre MR (2011) Geological foundation for production of natural gas resources from diverse shale formations: Sugarland, Texas, Research Partnership to Secure Energy for America Final Report 07122.17.01; Geological Survey of Alabama Open-File Report 1110, 156 p.

Pavlis, G. L., Vernon, F. L., Harvey, D., and Quinlan, D. (2004). The generalized earthquake location (GENLOC) package: A modern earthquake location library. *Computers in Geosciences* 30, p. 1079–1091.

Rabak, I., Langston, C., Bodin, P., Horton, S., Withers, M., and Powell, C. (2010). The Enola, Arkansas, Intraplate Swarm of 2001, *Seismol. Res. Lett.* 81, 549- 559.

Raleigh CB, Healy JH, Bredehoeft JD (1976) An experiment in earthquake control at Rangely, Colorado. *Science*, **191**, 1230–1237.

Rothert E, Shapiro SA (2007) Statistics of fracture strength and fluid-induced microseismicity. *Journal of Geophysical Research*, **112**, B04309.

Shapiro SA, Patzig R, Rothert E, Rindschwentner J (2003) Triggering of microseismicity due to pore-pressure perturbation: permeability related signatures of the phenomenon. *Pure Applied Geophysics*, **160**, 1051–1066.

Shapiro SA, Rothert E, Rath V, Rindschwentner J (2002) Characterization of fluid transport properties of reservoirs using induced microseismicity. *Geophysics*, **67**, 212–220.

Stanton G (1993) Processes and controls affecting anisotropic flow in the Boone-St. Joe aquifer in northwestern Arkansas. [M.S. Thesis]. Department of Geosciences, University of Arkansas, Fayetteville, Arkansas. 160 pp.

Talwani P, Chen L, Gahalaut K (2007) Seismogenic permeability, ks. *Journal of Geophysical Research*, **112**, B07309.

Theis CV (1935) The relation between the lowering of the piezometric surface and the rate and duration of discharge of a well using ground-water storage. *Transactions, American Geophysical Union*, **16**, 519–524.

Thurber, C. H. (1983). Earthquake locations and three-dimensional crustal structure in the Coyote Lake area, central California, *J. Geophys. Res.* 88, 8226.

Townend J, Zoback MD (2000) How faulting keeps the crust strong. *Geology*, **28**, 399–402.

Van Arsdale RB, Schweig ES (1990) Subsurface structure of the eastern Arkoma basin. *American Association of Petroleum Geologists Bulletin*, **74**, 1030–1037.

Warpinski, N. R., Du, J. and Zimmer, U. (2012). Measurements of Hydraulic-Fracture-Induced Seismicity in Gas Shales. *SPE Prod. Oper.*, **27**(3), 240–252.

Wiemer, S., and Wyss, M. (2002). Mapping spatial variability of the frequency–magnitude distribution of earthquakes, *Adv. Geophys*. 45, 259–302.

Zoback MD, Townend J (2001) Implications of hydrostatic pore pressures and high crustal strength for the deformation of intraplate lithosphere. *Tectonophysics*, **336**,19–30.

Zoback MD, Zoback ML (1991) Tectonic stress field of North America and relative plate motions. - In: Slemmons, DB, Engdahl ER, Zoback MD, Blackwell DD (eds.): Neotectonics of North America, 339-366.